



REPUBLIC OF INDONESIA

MINISTRY OF MINES

GEOLOGICAL SURVEY OF INDONESIA

REPORT ON GEOLOGICAL SURVEY
OF
CENTRAL KALIMANTAN

PHASE III (No. 2)

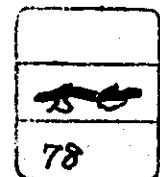
AIRBORNE MAGNETIC SURVEY

FEB. 1978

METAL MINING AGENCY OF JAPAN

JAPAN INTERNATIONAL COOPERATION AGENCY

GOVERNMENT OF JAPAN



108
66.1
MPN
14494

REPUBLIC OF INDONESIA
MINISTRY OF MINES
GEOLOGICAL SURVEY OF INDONESIA

REPORT ON GEOLOGICAL SURVEY
OF
CENTRAL KALIMANTAN

PHASE III (No. 2)
AIRBORNE MAGNETIC SURVEY

国際協力事業団	
受入 期日 843.92143	1080
登録No. 09626	66-112
	MPN->

FEB. 1978

JICA LIBRARY



1055343[6]

METAL MINING AGENCY OF JAPAN
JAPAN INTERNATIONAL COOPERATION AGENCY
GOVERNMENT OF JAPAN

P R E F A C E

The Government of Japan, in response to the request extended by the Government of the Republic of Indonesia, decided to conduct an integrated geological survey for mineral exploration in central Kalimantan of Indonesia, and commissioned its implementation to the Japan International Cooperation Agency.

The Agency, taking into consideration of the importance of technical nature of the survey work, in turn sought the Metal Mining Agency of Japan for its cooperation to accomplish the task within a period of four years.

The Government of the Republic of Indonesia appointed the Geological Survey of Indonesia to execute the survey as the counterpart to the Japanese team. The survey has been carried out jointly by both governments' experts.

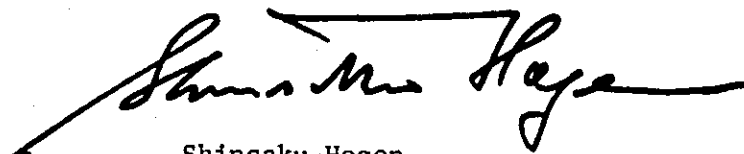
The first phase of the survey consists of Landsat data analysis; the second and third phase, aerial photography and airborne magnetic survey.

This report submitted hereby synthesizes the results of the second and third phase airborne magnetic surveys, and it will also form a portion of the final report that will be prepared with regard to the results obtained in the fourth phase.

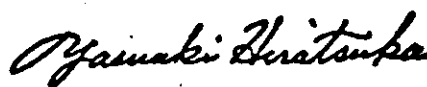
We wish to take this opportunity to express our gratitudes to all sides concerned with the excution of the survey.

February, 1978

Prof. Dr. J. A. Katili
Director general
Ministry of Mines
Republic of Indonesia



Shinsaku Hogen
President
Japan International
Cooperation Agency



Yasuaki Hiratsuka
President
Metal Mining Agency
of Japan

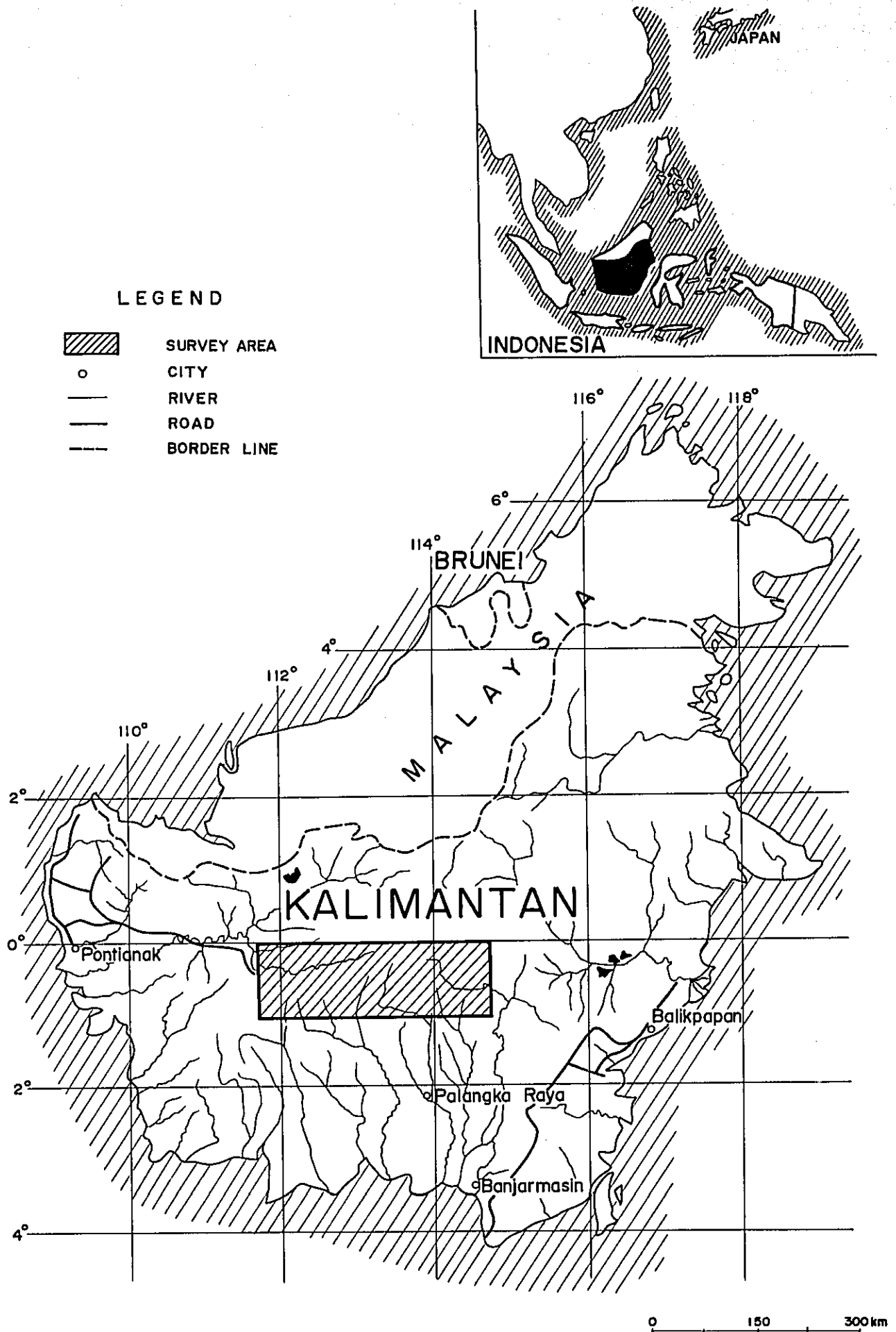


Fig.1 Location map of survey area

TABLE OF CONTENTS

	Page
PREFACE	1
LOCATION MAP OF SURVEY AREA	iii
ABSTRACT	1
Chapter 1 Introduction	4
1-1 Progress of survey	4
1-2 Purpose of survey	5
1-3 Outline of survey	5
1-4 List of members	6
Chapter 2 General Information	9
2-1 Location and accessibility	9
2-2 Topography	9
2-3 Climate and vegetation	9
2-4 Geology	11
Chapter 3 Airborne Magnetic Survey	15
3-1 Survey area and flight production	15
3-2 Survey period	15
3-3 Aircraft and instrumentation	20
3-4 Summary of field operations	25
3-4-1 Flight plan	25
3-4-2 Air base	26
3-4-3 Magnetic compensation of aircraft	28
3-5 Survey flight	28
3-6 Data processing	31
3-6-1 Preliminary data reduction and compilation	31
3-6-2 Data processing	36
3-7 Method of analysis	39
3-7-1 Spectral analysis	41
3-7-2 Second vertical derivative filter	44
3-7-3 Magnetic pole reduction filter	45
3-7-4 Quantitative analysis	47

	Page
3-8 Measurement of rock magnetism	50
Chapter 4 Survey Results	52
4-1 Residual map	52
4-2 Second vertical derivative map	55
4-3 Magnetic pole reduction map	57
4-4 Spectral analysis map	57
4-5 Quantitative analysis	60
Chapter 5 Summary of Results	62
Chapter 6 Conclusion	68
REFERENCES	70

LIST OF ILLUSTRATIONS

- Fig. 1 Location map of survey area
Fig. 2 Monthly precipitation in and around survey area
Fig. 3 Structural map of Kalimantan
Fig. 4 Modified geological column
Fig. 5 Airport in Kalimantan
Fig. 6 Flight altitude map
Fig. 7 Flow chart of data processing and analysis
Fig. 8 Lattice configuration for second vertical derivative calculation
Fig. 9 Lattice configuration for magnetic pole reduction calculation
Fig. 10 Sectional map of survey area
Fig. 11 Energy spectrum vs. frequency

- Table 1 Results of surveys in Kalimantan
Table 2 List of effective flight lines (Phase II, 1976)
Table 3 List of effective flight lines (Phase III, No. 1, 1977)
Table 4 List of effective flight lines (Phase III, No. 2, 1977)
Table 5 List of survey flight hours (Phase II, 1976)
Table 6 List of survey flight hours (Phase III, No. 1, 1977)
Table 7 List of survey flight hours (Phase III, No. 2, 1977)
Table 8 Aircraft inspection schedule
Table 9 IGRF geomagnetic component in central Kalimantan (1977.5)
Table 10 Susceptibilities of rock samples
Table 11 Results of qualitative analysis

PL. I	Residual map	(scale 1:250,000)
PL. II	Second vertical derivative map - 1	(scale 1:250,000)
PL. III	Second vertical derivative map - 2	(scale 1:250,000)
PL. IV	Magnetic pole reduction map	(scale 1:250,000)
PL. V	Spectral analysis map (Deep effects)	(scale 1:250,000)
PL. VI	Spectral analysis map (Shallow effects)	(scale 1:250,000)
PL. VII	Interpretation map	(scale 1:250,000)
PL. VIII	Airborne magnetic tectonic profile	(scale 1:250,000)

A B S T R A C T

The airborne magnetic survey has been conducted as a part of the integrated geological survey project in the central Kalimantan, the Republic of Indonesia, with a purpose of clarifying the geological structures and igneous rock distribution in pursuit of possibilities of ore deposits in the survey area.

This report summarizes the results of the airborne magnetic survey executed during the period from 1976, the second year of the project, to 1977.

Judging from the obtained magnetic features, the survey area is divided into three parts : i.e. 1) the low magnetic anomalies of long wavelength in the Northwestern Part of the survey area, 2) the extremely high magnetic anomalies of short or medium wavelength in the Southwestern Part of the survey area, and 3) the Eastern Part of the survey area having a mixed characteristic feature of the above two parts.

It is concluded on the basis of magnetic measurements of rock samples that the extremely high magnetic anomalies may be caused by andesite and dioritic rock, on the other hand, the weak magnetic anomalies may be distributed in relation to sandstone, mudstone, shale, etc.

The magnetic analyses with the results of the rock-magnetic measurements and available geological data come to the following

conclusions of igneous rock distribution and possibilities of ore deposits.

- 1) Granitic rocks forming the basement structure extend in the direction of WNW-ESE over the Southwestern Part of the survey area and ENE-WSW over the Central Part. It is presumed that the structure reaches the northeastern and southeastern borderlines of the Eastern Part.
- 2) Sedimentary rocks, such as sandstone, mudstone, shale, etc. are distributed in the direction of E-W over the Northwestern Part of the survey area. It is presumed that they form thick layers in the eastern section of the Northwestern Part.
- 3) The predominant distribution of andesitic rocks is found in the Eastern Part.
- 4) The magnetic feature is well consistent with the basement structure with WNW-ESE trending magnetic structural lines in the western part and NE-SW trending magnetic structural lines in the eastern part of the survey area.
- 5) The basement structure and the major magnetic structural lines turn their trends in the southern section of the Central Part, where the magnetic feature reflects the complex geology including a number of fault lines.
- 6) The mineralized zones promising for ore deposits are found in the southern section of the Central Part by the geological survey. The corresponding mineralization is presumed to have a relation with the Tertiary granite. Although the exact

distribution of the Tertiary granite is not clarified from the present survey, it is probably true that, judging from the complex geology of the southern section of the Central Part as mentioned in 5), the geological condition of forming the mineralization related Tertiary granite is satisfied there.

For the next-year program of the project, the further geological survey together with geochemical exploration is deeply desired to be concentrated into the south of the Central Part for the purpose of selecting ore-promising spots.

Chapter 1 Introduction

1-1 Progress of survey

The integrated geological survey was launched in central Kalimantan as a technical cooperation project between the Republic of Indonesia and Japan in 1974. The airborne magnetic survey formed a part of the project. In the initial year of the project, the Landsat data analysis was set up to clarify topography, forestry, geology and geological structure over the survey area. In the second year, the aerial survey was conducted to prepare aerial photographs for airborne magnetic and geological surveys and photogeological interpretations, and covered 71% of the whole area. The airborne magnetic survey was conducted in the same year to cover about 25 % of the whole area. In the third year, the remaining parts of the area have been successively surveyed by these methods to cover 22 % (aerial photography) and 70 % (airborne magnetic survey). The progress of the surveys is summarized in Table 1.

Table 1 Surveys in Kalimantan

Item	Year	1975 (phase I)	1976 (phase II)	1977 (Phase III)	
				No.1	No.2
1 Landsat data analysis		100 %			
2 Aerial photography			71 %	22 % total 93 %	
3 Airborne magnetic survey			about 25 %	29 % total 54 %	41 % total 95 %

1-2 Purpose of survey

The airborne magnetic survey was executed to clarify the geological structure, such as igneous rock distribution promising for an ore deposit.

1-3 Outline of survey

The airborne magnetic survey was conducted in 1976 and 1977 as a part of the integrated geological survey in Central Kalimantan. The total area amounts to about 36,300 km², ranging from latitude 0°00' to 1°00' S, and longitude 111°45' to 114°45' E. The survey was originally planned to start in May 1976 to cover about 50 per cent of the whole area. However, the survey aircraft Cessna 402B PK-VCD experienced a main landing gear collapse on 12th May, at Jakarta during the test flight. Due to the aircraft accident, the survey was started in early August by substituting another aircraft Cessna 402B PK-VCE, finally to cover about 25 per cent of the whole area until an interruption of the survey due to bad weather on 23rd October. The 1977 survey was started on 19th March to complete the remaining part and covered about 70 per cent of the whole area by the end of June. On 7th July, the survey aircraft returned to Palangka Raya survey base after completing the second 100-hour cycling inspection, while on a landing roll of the Panarung airport, Palangka Raya, the aircraft experienced again a main landing gear collapse. It was reported that the repair of the aircraft would require about two months at least. Considering the time requirement for repair and also the fact that the survey had already been completed over about 95 per cent of the whole area, both Indonesian

and Japanese Governments agreed to stop the survey at this stage.

The data obtained from the survey was preliminary processed at the survey base and at Geological Survey of Indonesia. The data processing through computer and the interpretation works were made in Japan. The part of the computer processings and data analyses were jointly carried out by the staff of the Geological Survey of Indonesia and the members of Japanese survey team.

1-4 List of members

The members engaged in the project works are listed herein.

Airborne magnetic survey in 1976

Indonesian team	Japanese team
	Supervisor
	Nobutaka Miyazoe (MMAJ)
	Masaharu Kaneko (MMAJ)
	Toshio Kawaguchi (MMAJ)
	Yutaka Hatano (JICA)
Coordinator	Coordinator
Adjat Sudradjat (GSI) Chief of photogeology section	Haruhiko Hirayama (NED) Team leader, Geologist
Survey members	Survey members
Soetijoso Djojomihardjo (GSI) Geophysicist	Kenichi Nomura (NED) Geophysicist
Marzuki Sani (GSI)	Masao Yoshizawa (NED) Geophysicist
Kastidjo Mardjo (GSI)	Tamotsu Fujikawa (NED) Electrotechnician
Aircraft crew (PENAS)	Ikuo Takahashi (NED) Dataman

Airborne magnetic survey in 1977

Indonesian team	Japanese team
	Supervisor
	Nobutaka Miyazoe (MMAJ)
	Keiichi Takeda (JICA)
Coordinator	Coordinator
Adjat Sudradjat (GSI) Former chief of photogeology section	Haruhiko Hirayama (NED) Team leader, geologist
Survey members	Survey members
Mohamad Untung (GSI) Chief of geophysical research section	Kenichi Nomura (NED) Geophysicist
Soetijoso Djojomihardjo (GSI) Geophysicist	Tamotsu Fujikawa (NED) Electrotechnician
Sardjono (GSI) Electrotechnician	Ikuo Takahashi (NED) Dataman
Nana Komara (GSI) Draftsman	
Basuki Sugiharto (GSI) Draftsman	
Nano Suparno Geophysical operator, measurement of susceptibility	
Bundan Mubroto (GSI) Geophysicist	
Aircraft crew (PENAS)	
Cooperator (Japanese experts attached to GSI)	
Sakae Ichihara (JICA)	
Mitsuharu Yako (JICA)	

On the basis of the natural resources development program and the request of the Indonesian Government, the survey was conducted in cooperation with Indonesian aerial survey company Perusahaan Umum Survai Udara.

Note :	GSI	Geological Survey of Indonesia
	JICA	Japan International Cooperation Agency
	MMAJ	Metal Mining Agency of Japan
	NED	Nikko Exploration and Development Co., Ltd.
	PENAS	Perusahaan Umum Survai Udara

Chapter 2. General Information

2-1 Location and accessibility

The survey area covered by the airborne magnetic survey is located in central Kalimantan as shown in Fig. 1.

In the survey area, no large villages exist but only small villages are scattered about along the rivers.

There are very few roads along the rivers in east and west parts of the area. The area still remains undeveloped as a whole and the rivers are major means of transportation.

2-2 Topography

The greater part of the survey area is located in a comparatively lowland area comprising plains of 100 m to 500 m in altitude. The mountain ridges extend from southwest to north in the center of the area and the highest peak reaches 2,278 m (Mt. Raja) in altitude.

As for water system, in an area ranging from east to southwest, water flows predominantly in a north-south direction and consists of the main streams and several branches of the Barito River. In the northwest part of the area, the main water system is composed of the Melawi River, flowing to the west, and of its branches.

2-3 Climate and vegetation

The climatic condition is characterized by high temperature and high humidity because of the area situating close to the equator and in a zone of moderate altitude (except for a part of the area).

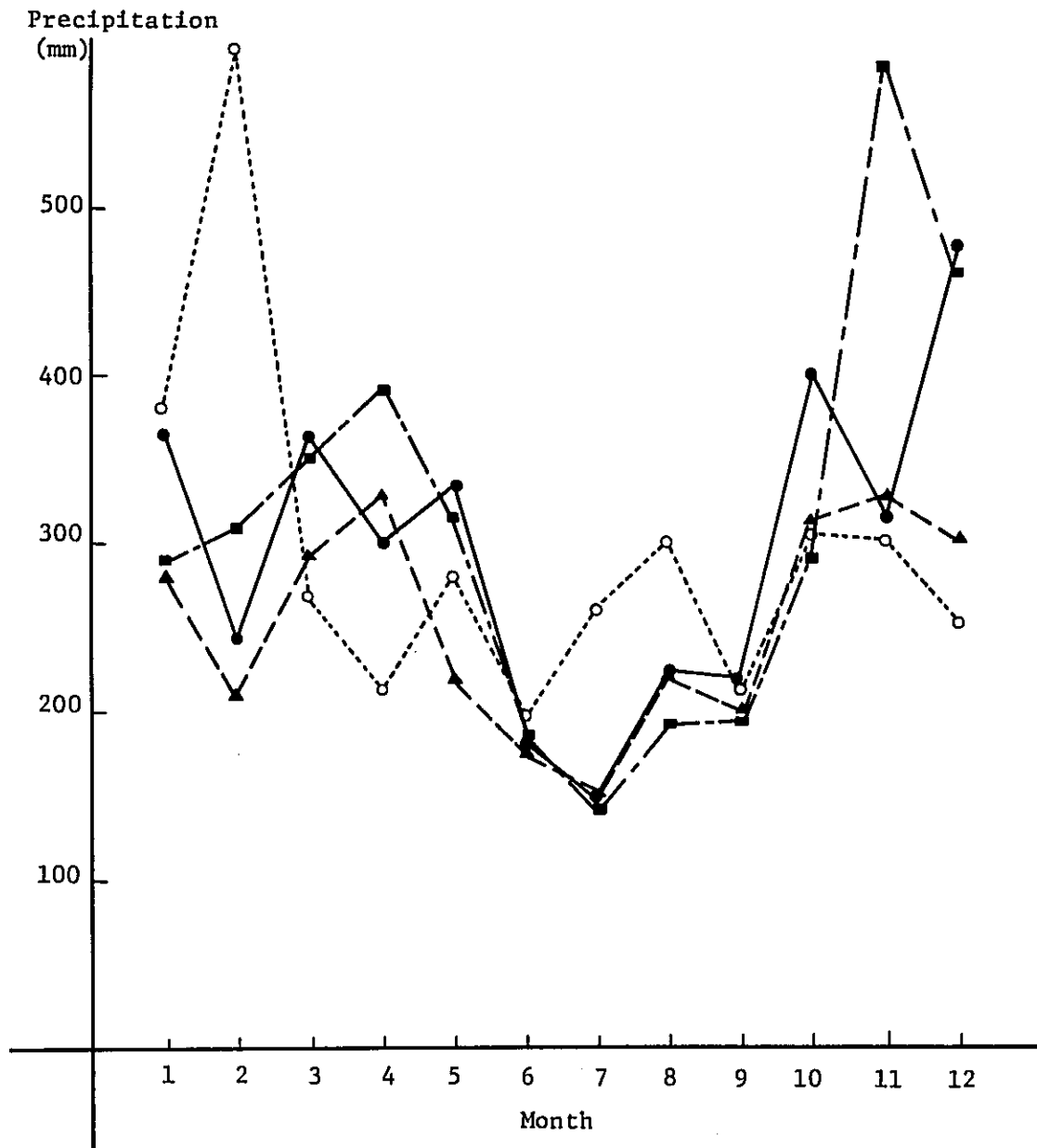
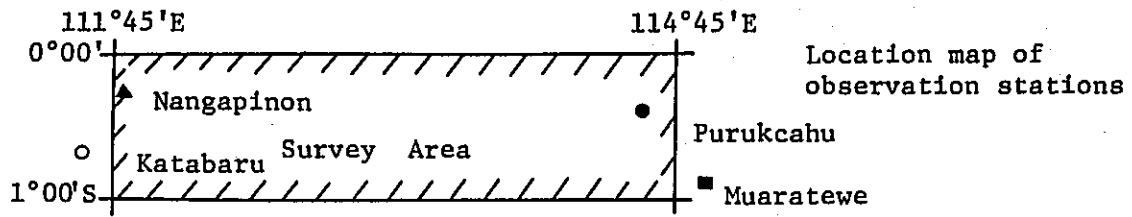


Fig. 2 Monthly precipitation in and around survey area (mean values from 1963 to 1974)

In Balikpapan and Pontianak, the seaside cities, located at almost the same altitude as the survey area, the annual average temperature and humidity reaches 26 - 28°C and 75 - 80 per cent respectively.

A year is typically divided into the dry season, June to September, and the wet season, October to May. As shown in Fig. 2, precipitation varies according to places of observation. Generally, however, the monthly precipitation registers 200 to 300 mm during the dry season but 300 to 400 mm during the wet season, totaling 3,000 to 4,000 mm in annual precipitation. The precipitation data shows that the area is abundant in rainfall throughout the year. The area is mostly a tropical jungle.

2-4 Geology

The survey area is situated in the northern margin of the Sunda Shield and the Tewah High uplifted belt, and the southern margin of the Melawi Basin, as shown in Fig. 3.

A geological map of 1 : 500,000 scale was published by the Geological survey of Indonesia. According to the map the southern part of the survey area consists mainly of Carboniferous to Triassic formations with acidic to intermediate intrusive bodies, the northern part of Pliocene to Pleistocene units, and the southeastern part of Eocene to Miocene formations. Carboniferous to Triassic and Cretaceous units are shown in the north of the survey area, although the lithology of these units is not shown in the map. The Pliocene to Pleistocene formations in the northern part are considered to be controlled by the east-west trending fold structure, while in the south the geological structure is not clear. According to the data by Geological Survey of

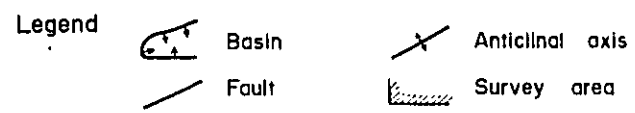
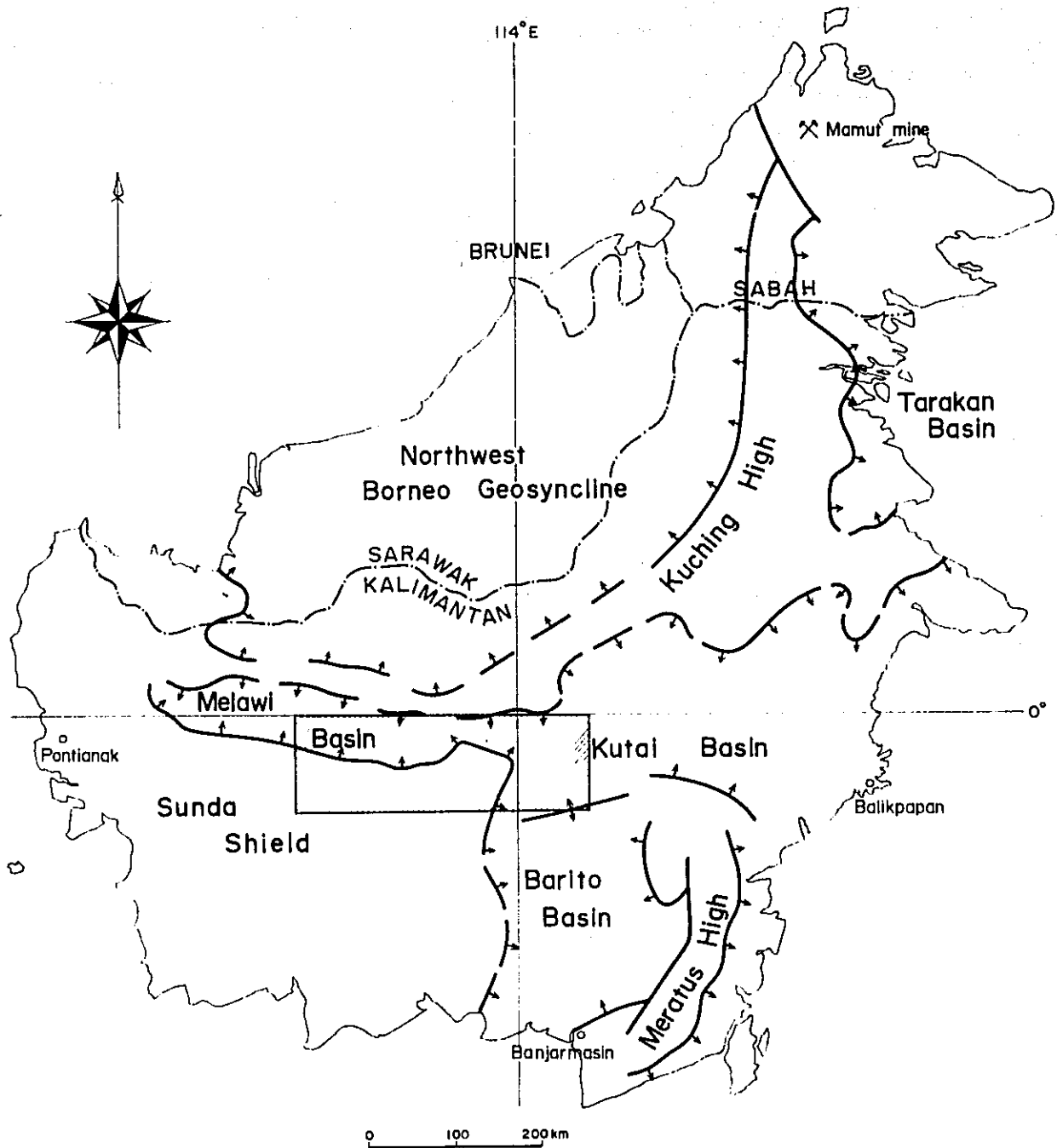


Fig.3 Structural map of Kalimantan

Indonesia, the geology of Kalimantan consists mainly of Tertiary to Quaternary formations deposited on the Melawi Basin in the west, Barito Basin in the south, and Kutai Basin in the east. The Carboniferous to Triassic units form the basement of these basins together with the Cretaceous system (see Fig. 4). The petroleum has not been found in the Melawi Basin contrary the fact that large oil fields are known in both the Barito and Kutai Basins.

Age	Column	Descriptions
Alluvium		Alluvial Deposits Laterites
Pleistocene		Basalts
		Andesites Coarse-Sandstones
Pliocene		Sandstones Fine-Sandstones
Miocene		Alternation Limestones of Shales and Sandstones
		Tuffs Pyroclastic rocks
Paleocene		Intrusive rocks
Cretaceous		Andesites
Triassic		Metamorphic rocks Metasedi- ments
Carboniferous		Granites

- Notes :
1. Lineament patterns of Units M and D are different from Units N to B.
 2. Folding structures are observed in Units E, T, H and C.
 3. Bedding planes of Units C, F, S and B are nearly flat.

Fig. 4 Modified geological column

Chapter 3 Airborne Magnetic Survey

3-1 Survey area and flight production

The area covered by the airborne magnetic survey is located in central Kalimantan as shown in Fig. 1.

The total area amounts to about 36,300 km² ranging from latitude 0°00' to 1°00' S, and longitude 111°45' to 114°45'E.

The area surveyed in 1976 occupies the northwest and central parts of the above area, about 25 per cent of the whole area with effective flight line extension of 3,606 km. In 1977, the survey was successively carried out to cover the remaining part with an effective flight line extension of 9,144.9 km. Totaling the surveys in 1976 and 1977, 95 per cent of the whole area was covered with the flight lines of 12,750.9 km in length (see Tables 2, 3 and 4).

3-2 Survey period

The general time schedule was set up as follows:

Airborne magnetic survey in 1976 (Phase II)

April 30 to May 11, 1976 :	Mobilization and preparatory works
May 12, 1976 :	Aircraft accident (failure in landing during the test flight due to trouble of landing gear)
May 13 to August 6, 1976 :	Arranging for substitute aircraft
August 7 to October 23, 1976 :	Airborne magnetic survey
October 24 to November 5, 1976 :	Arrangements and compilation of data, Demobilization

November 6, 1976 to January 31,
1977 : Report (Phase II)

Airborne magnetic survey in 1977 (Phase III No. 1 and No. 2)

Phase III No. 1

March 8 to March 18, 1977 : Mobilization and preparatory works
March 19 to May 26, 1977 : Airborne magnetic survey
May 27 to July 31, 1977 : Report (Phase III No. 1)

Phase III No. 2

May 27 to July 6, 1977 : Airborne magnetic survey
July 7, 1977 : Aircraft accident (failure in land-
ing due to trouble of landing gear)
July 8 to July 27, 1977 : Arrangements and compilation of
data, Demobilization
July 28, 1977 to February 15,
1978 : Report (Phase III No. 2)

Table 2 List of effective flight lines (Phase II, 1976)

Traverse lines

Planned Line No.	Flight Line No.	Production km	Planned Line No.	Flight Line No.	Production km
T- 1	T- 1	80.8	T- 26	T- 26	73.7
2	2	61.2	27	27	71.5
3	3	42.7	28	1028	69.6
4	4	88.9	29	29	72.4
5	5	77.0	30	1030	73.3
6	6	50.6	31	31	73.5
7	7	70.0	32	1032	65.5
8	8	68.8	33	1033	60.8
9	9	73.4	34	34	70.9
10	10	80.6	35	35	69.3
11	11	84.9	36	36	60.0
12	12	79.7	37	2037	59.0
13	13	82.3	38	38	58.5
14	14	75.4	39	39	58.7
15	15	76.7	40	40	57.3
16	16	78.2	41	41	59.8
17	1017	71.3	42	42	111.0
18	18	67.7	43	43	111.0
19	1019	66.5	44	44	35.7
20	20	70.1	45	45	76.7
21	21	59.3	78	78	111.0
22	22	71.3	80	80	111.0
23	23	76.1	81	81	111.0
24	24	75.5	84	84	80.0
25	25	75.8			
				Total	3,606.0 km

(*) Total effective flight line length of traverse lines in Phase II is 3,606 km.

Table 3 List of effective flight lines (Phase III No. 1, 1977)

Traverse lines

Planned Line No.	Flight Line No.	Production km	Planned Line No.	Flight Line No.	Production km
T- 65	T- 62	111.0	T- 93	T- 92	111.0
66	63	111.0	95	93	111.0
67	64	111.0	96	96	111.0
68	65	111.0	99	1097	111.0
69	66	111.0	101	101	111.0
70	67	111.0	102	2102	111.0
71	1069	111.0	103	102	56.0
72	71	111.0	"	1103	55.0
73	72	111.0	104	102	55.0
74	73	111.0	105	105	111.0
75	74	111.0	106	106	111.0
77	1076	111.0	107	107	111.0
86	85	56.0	108	108	45.0
87	85	55.0	109	108	55.0
88	1087	111.0	110	112	90.0
89	88	111.0	"	1110	21.0
91	1089	111.0	112	1112	70.0
92	91	111.0	Subtotal		3,333.0 km

Tie lines

Planned Line No.	Flight Line No.	Production km	Planned Line No.	Flight Line No.	Production km
C-5002	C-7002	140.0	C-5003	C-6003	140.0
Subtotal				280.0 km	

(*) Total effective flight line length of traverse and tie lines in Phase III No. 1 is 3,613 km.

Table 4 List of effective flight lines (Phase III No.2, 1977)

Traverse lines

Planned Line No.	Flight Line No.	Production km	Planned Line No.	Flight Line No.	Production km
T- 1	T-2001	30.2	T- 45	T-1044	34.3
2	1002	49.8	46	46	56.0
3	2003	68.3	47	46,1047	111.0
4	1004	22.1	48	47	111.0
5	1005	34.0	49	48	111.0
7	1007	41.0	50	49	111.0
8	1008	42.2	51	1050	111.0
9	1009	37.6	52	50	111.0
10	1010	30.4	53	52	111.0
11	1011	26.1	54	53	111.0
12	2012	31.3	55	1054	111.0
13	1013	28.7	57	1055	111.0
14	1014	35.6	58	2057	111.0
15	1015	34.3	59	55	111.0
17	1017	39.7	60	56	111.0
18	2018	43.3	61	1057	111.0
19	2019	44.5	62	59	111.0
20	1020	40.9	63	1060	111.0
21	1022	51.7	64	61	111.0
23	1023	34.9	79	2078	111.0
24	1024	35.5	82	2081	111.0
25	1026	35.2	83	82	111.0
26	1027	37.3	84	83	31.0
27	2027	39.5	85	1085	111.0
29	1029	38.6	86	86	55.0
30	2030	37.7	87	3087	56.0
31	1031	37.5	94	94	111.0
33	3033	50.2	97	3097	111.0
34	1035	40.1	98	2098	111.0
35	2035	41.7	100	100	111.0
36	1036	51.0	104	2104	56.0
37	3037	52.0	108	2108,3108	66.0
38	1038	52.5	109	109	56.0
39	1039	52.3	111	111	111.0
40	2040	53.7	112	3112	41.0
41	1041	51.2	Subtotal		4,809.9 km

Tie lines

Planned Line No.	Flight Line No.	Production km	Planned Line No.	Flight Line No.	Production km
C - 5001	C-5001,6001	334.0	C - 5003	C - 7003	194.0
5002	8002	194.0	Subtotal		722.0 km

(*) Total effective flight line length of traverse and tie lines in Phase III No.2 is 5,531.9 km.

3-3 Aircraft and instrumentation

The aircrafts used for the survey were a twin-engined Cessna 402B-registration number PK-VCE in 1976 and PK-VCD in 1977, equipped with a tail stinger for airborne survey. The PK-VCD was equipped with a Doppler navigation system.

The instrumentation used for the survey was as follows :

a. A Gulf Mark III Fluxgate Magnetometer. This magnetometer is a fluxgate instrument for measuring variations in earth's magnetic field with a resolution of 1 gamma. The fluxgate magnetometer makes use of a ferromagnetic element of such high permeability that the earth's field can induce a magnetization that is substantially proportional to its saturation value. If the earth's field is superimposed upon a cyclic field induced by an alternating current in a coil around the core, the resultant field will saturate the core at each half cycle of the current flow. The phase in each cycle at which saturation is reached depends upon the sum of difference between the ambient field and the strength of the imposed alternating field.

In practice, two parallel cores are aligned with their axes in the direction of the earth's field. Identical primary windings in series magnetize the two cores with the same flux density but in opposite directions, since their coil windings are opposite around the respective cores. Accordingly, the earth's field reinforces the field of one coil but opposes that of the other. In the Gulf Mark III airborne magnetometer, a compensating coil is set up to cancel an unbalancing effect of the ambient field which is caused by unbalance in the two coils. The current flowing through this

coil is recorded on a self balancing moving type potentiometer recorder, and supplies a precise measure of the amount of the ambient field.

The orienting system automatically keeps the above-described measuring elements parallel with the earth's total magnetic field by feedbacking the output of two fluxgates on the support platform to the actuate orienting servo systems.

The sensor head is installed in a tail stinger on the rear of the aircraft.

b. A GeoMetrics Airborne Proton Magnetometer, Model G-803.

This proton free precession magnetometer operates on the principle of nuclear magnetic resonance to measure the earth's total magnetic intensity. In the proton magnetometer sensor, a uniform magnetic field is created by passing a few amperes of current through a coil about a small volume of proton-rich hydro-carbon fluid such as water or kerosene. The spinning protons act as small magnetic dipoles and align themselves with the applied field. When the field is removed, the protons precess in phase about the direction of the earth's field at a rate proportional to the total magnetic intensity. This rate, or Larmor precession frequency, is determined by the gyromagnetic ratio of the proton (23.4874 gammas per Hz). The precession frequency is independent of the direction of the spins with respect to the earth's field; only the signal amplitude varies, being maximum when the spins are normal and zero when they are parallel to the direction of the earth's magnetic field. The frequency of the precession signal, as determined by the gyromagnetic ratio, has a rate of 0.04 Hz per gamma, ranging from 1,250 to 3,400 Hz,

i.e. from 30,000 to 80,000 gammas in the earth's magnetic field. In the present survey, a sampling rate of the magnetometry was selected as 0.8 seconds with an accuracy of 0.5 gammas.

c. A Gulf Magnetic Storm Monitor. This storm monitor is a fluxgate type magnetometer with an accuracy of 2 gammas.

d. A Geometrics Base Station Monitor Proton Magnetometer, Model G-806. This proton magnetometer measures the earth's total magnetic field with a 1-gamma sensitivity. This magnetometer and Gulf fluxgate storm monitor above mentioned were respectively used for dual purposes to correct the daily magnetic variations in the airborne magnetic data, and to monitor the magnetic storms during flight.

e. A Honeywell Radar Altimeter, Type AN/APN 171. This altimeter is a pulse type echo-tracking radar unit designed for accurate altitude terrain clearance measurements. It consists of a Receiver-Transmitter and two antennas. Transmitter operates at 4,300 megahertz. High resolution tracking is maintained in an altitude range of 0 to 5,000 feet. Height is displayed on a pilot's indicator and the analogue signal is provided to an external recording equipment. The antenna pattern is relatively wide, $\pm 35^\circ$ so that in rugged terrain the instrument will track features such as cliff sides etc., if these are nearer than the ground below the aircraft.

f. A Barometric Altimeter.

The barometric altimeter was used to keep a constant barometric

altitude for the navigation of the aircraft. In the survey, the aircraft was navigated constantly at a height of 2,000 m.

g. Two-channel Hewlett Packard Analogue Recorders, Models 7130A and 7100B.

These recorders were used to record the following data in real time :

- i) Magnetometer (total magnetic intensity)
- ii) Doppler radar (along track and across track)
- iii) Radar altimeter (altitude from the ground)

The recorders are devised to record fiducial marks at intervals of 10 seconds for the synchronization of the above described data with tracking film. In the survey, magnetic data were recorded on a chart with full scale of 50 gammas. The chart speed of the recorders was 2 in./min.

h. A NAC 35 mm Tracking Camera, Model ST-1000. This continuous strip camera is used to determine the flight path with the following features :

- i) Variable film speed 1 to 7 mm per minute
- ii) Remotely operated aperture control
- iii) Two film footage counters
- iv) Two independently operated fiducial markers
- v) Film break cut-out switch
- vi) Operates with 400 ft. magazines

In the survey, 400 ft. film was charged at a speed of 2 mm per second.

i. A Bendix Doppler Navigation System Type DRA-12, CPA-24. This Doppler system was employed for navigation guidance and flight path recovery. The Doppler Navigation System consists of DRA-12 Doppler Radar System and CPA-24 Navigation Computer System. The Doppler Radar System consists of Frequency Tracker and Transmitter-Receiver. The purpose of the tracker is to convert the outputs of the Transmitter-Receiver into useful information indicating the aircraft ground speed and drift angle by means of the system indicators. The Navigation Computer System converts ground speed and course-made-good information, supplied by a Doppler Radar System, into digital readouts representing 1) distance in nautical miles (left or right) from a selected course and 2) distance in nautical miles from a selected designation.

This Doppler Navigation System has the following characteristics :

Doppler type	FM/CW
Ground speed and drift angle computation	Digital
Operating frequency	8,800 mc
Transmitter power	0.5 watt
Pitch limit	up to 45° (depending on altitude and terrain)
Roll limit	up to 60° (depending on altitude and terrain)
Drift angle limit	$\pm 40^\circ$
Ground speed limit	100 to 999 knots
Drift angle error	0.25° (for 95% of observations)
Ground speed error	0.3 % (for 95% of observations)

Altitude	0 to 50,000 feet in reserve
Navigation computer accuracy	Along track : less than 0.5 % or 1 nm error (whichever is greater) Cross track : with perfect heading reference, less than 0.5 % or 0.1 nm error (whichever is greater)
Typical system operating accuracy	1 % of distance navigated

j. An N-1 Compass System. This N-1 compass system is a remote-indicating magnetic-slaved, directional gyro-stabilized compass system, designed for an airborne use in all latitudes. It may be operated either as a magnetic-slaved compass or as a directional gyro. In either mode, directional reference information is available for Doppler or other equipment. The maximum drift error in the free-gyro mode is $\pm 1.5^\circ$ per hour.

All the data obtained in the course of a flight was synchronized by fiducial signals coming out of a High-accuracy Seiko Digital Clock at constant intervals of 10 seconds.

3-4 Summary of field operations

3-4-1 Flight plan

Main specifications for the airborne magnetic survey were as follows:

Flight altitude :	2,000 m above sea level (except mountainous zones of 1,800 m or higher in altitude)
Flight direction :	Traverse line : North-south Tie line : East-west

Flight line spacing : Traverse line : 3 km
Tie line : 40 km

3-4-2 Air base

The airport used for the survey is Panarung Airport in Palangka Raya, about 150 km south of the survey area (see Fig.5). The airport has a 1,500 m long and 30 m wide asphalt-paved runway and a radio beacon which permitted safe take-offs and landings even when the weather is bad to some extent. As Panarung Airport had no facilities for fuel supply, aviation fuel and lubrication oil was transported from Jakarta to Palangka Raya via Banjarmasin by a cargo boat and a barge.

For periodic overhauls of the aircraft, the 50- and 100-hour cycling inspections were made at Palangka Raya and Banjarmasin respectively.

Name of Airport	Location	Size of Airstrip (m)	Airstrip Condition
Balikpapan	1.15°S 116.50°E	1,800	Asphalt-paved
Banjarmasin	3.22°S 114.33°E	1,775	Asphalt-paved
Batu Licin	3.00°S 116.00°E	900 x 12	Asphalt-paved
Muaratewe	0.57°S 114.54°E	600 x 20	Grass
Palangka Raya	2.16°S 113.56°E	1,500 x 30	Asphalt-paved
Pangkalanbuun	2.45°S 111.40°E	1,800 x 45	Grass
Pontianak	0.05°S 109.16°E	1,600	Asphalt-paved
Sampit	2.31°S 112.59°E	500 x 12	Grass
Sintang	0.04°S 111.29°E	557 x 30	Grass
Tanjung Warukin	2.13°S 115.26°E	1,300 x 30	Asphalt-paved

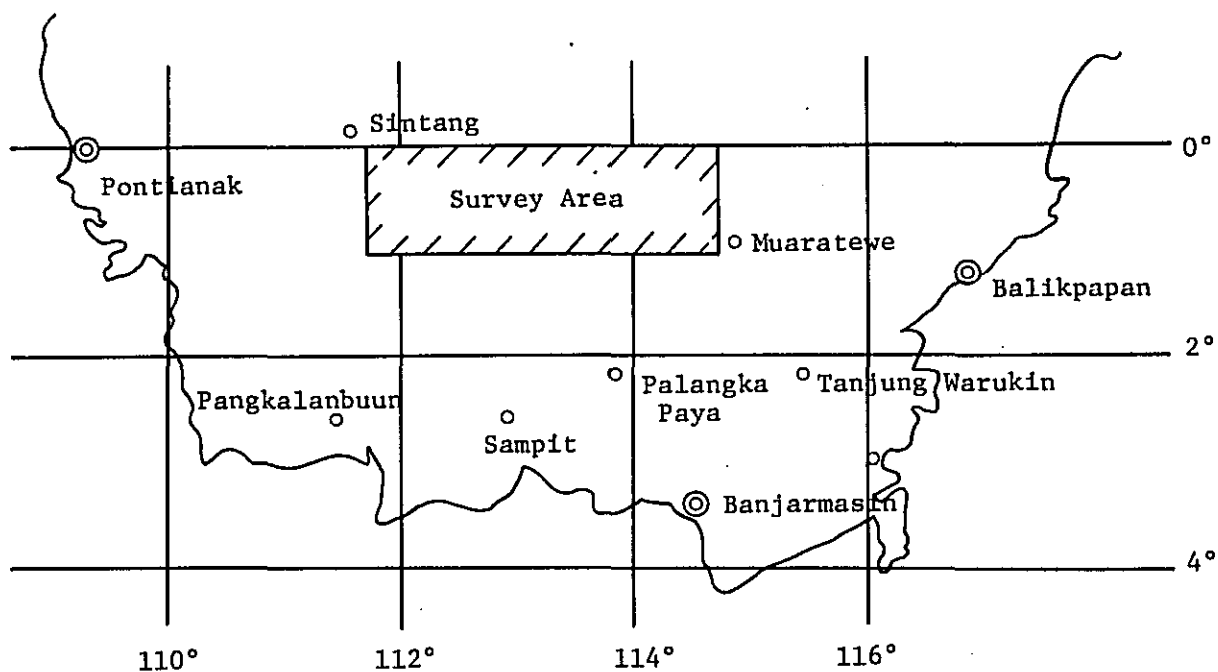


Fig. 5 Airport in Kalimantan

3-4-3 Magnetic compensation of aircraft

Possible causes of magnetic interference for aircraft inboard installations are as follows :

The first is the remanent magnetism of the various aircraft parts made of steel such as engines. The second is the magnetic field induced to these parts due to magnetic susceptibility through the earth's magnetic field. The third is the magnetic effect of eddy currents generated in the skin and other conducting parts of the aircraft by their motion in the earth's magnetic field.

In the survey, the aircraft-remanent magnetism was compensated at Panarung Airport by the use of a set of three-orthogonal compensating coils, mounted in the stinger. After the adjustment the relationship between aircraft facing directions and magnetic readings became as follows :

South-facing	42,225 gammas
North-facing	42,224 gammas
East-facing	42,202 gammas
West-facing	42,202 gammas

3-5 Survey flight

The 1976 survey flight was started from the northwest part of the survey area, including the range contoured with a comparatively high accuracy in the topographic map of 1/250,000 scale.

The 1977 survey flight was started from the eastern part of the survey area. The navigation was maintained by the use of a Doppler

navigation system with 1/250,000 scale topographic maps (printed by the Army Map Service, sheet numbers 12/VI, 12/VII, 12/VIII, 13/VI, 13/VII, 13/VIII), photomosaics of LANDSAT imagery and SLAR (Side Looking Airborne Radar) imagery and a 1/40,000 scale photomosaic of aerial photographs.

The length of traverse lines flown in the north-south direction amounted to 111 km at a standard line spacing of 3 km. The tie lines were flown in the east-west direction. According to the original plan, the standard spacing of tie lines was 40 km, but in actuality, in the eastern part of the survey area, the central tie line was shifted about 10 km to the north and the southern tie line was shifted about 5 km to the south from the planned location. Accordingly, the actual line spacing became 55 km. To complete the specification, an additional tie line was set up in between the preceding tie lines.

The flight altitude of the survey was maintained at a constant height of 2,000 m above sea level, except mountainous zones of 1,800 m or higher in altitude. The areas exceeding 2,000 m in flight altitude are shown in Fig. 6. Flight speed of the aircraft was approximately 140 knots throughout the survey.

During the survey flights, daily magnetic variations were continuously recorded at the Panarung Airport base station. No magnetic storm causing conspicuous magnetic change was observed during the survey flights.

The elements of the earth's magnetic field in the survey area are as follows.

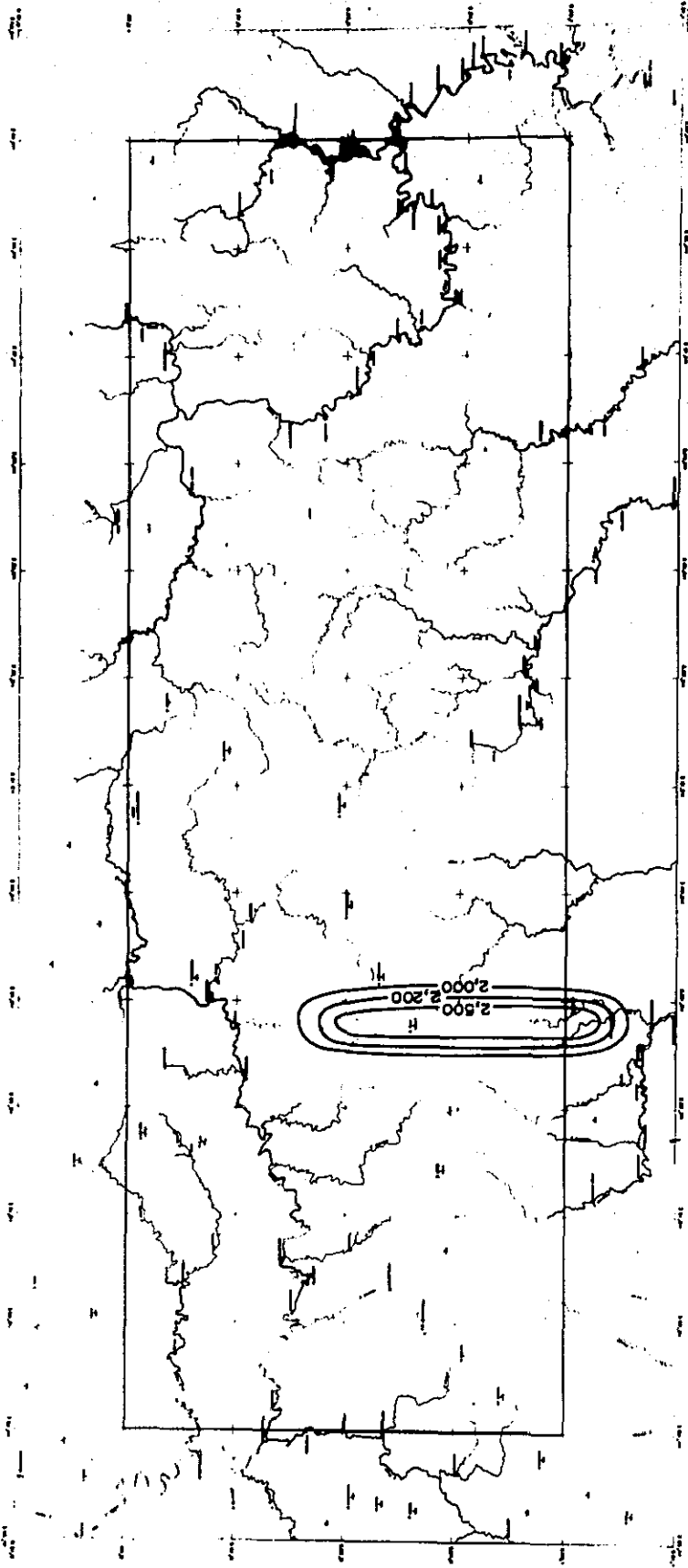


Fig. 6 Flight altitude map (contours indicate areas exceeding 2,000 m above sea level in flight altitude)

Total intensity : 41,700 gammas
Inclination : -20°
Declination : 2°E

The survey flight hours and aircraft inspection schedule are summarized in Tables 5,6,7 and 8.

3-6 Data processing

3-6-1 Preliminary data reduction and compilation

The following preliminary data processing works were carried out in Palangka Raya.

- 1) After every flight the tracking films were developed and dried up on the same day.
- 2) Using the developed tracking films, survey flight paths were plotted on an uncontrolled photomosaic assembled from the aerial photographs of approximately 1/40,000 scale.
- 3) The flight paths were transcribed into topographic maps of 1/250,000 scale with an auxiliary use of Doppler record in the case that no obvious landmark was found on the maps. In the course of the survey flights, it was found that these topographic maps were greatly distorted in some areas. For such areas, SLAR imagery and LANDSAT imagery photomosaics of 1/250,000 scale, which were considered to be comparatively reliable, were used for the flight path recovery in the survey.

Table 5 List of survey flight hours (Phase II, 1976)

Date	Hour	Remarks	Date	Hour	Remarks	
August 7	5.00	Mobilization to Palangka Raya Survey flight start	September 14	4.40		
8	2.30		15	3.50		
9	1.10		16	4.40		
10	2.00		17	1.15		
11	2.40		18	6.00		
12	2.10		19	7.25		
13	3.30		20	5.50		
14	3.10		21	2.30		
15	5.05		22	0.50		
16	4.00		24	8.10		
17	0.45		26	2.55		
18	3.25		27	3.40		
21	2.10		28	2.05		
22	2.15		29	2.25		
23	5.15		30	2.30		
24	5.10		Subtotal	86.25		(September)
25	1.30		October 1	1.20		
26	5.10		2	1.20		
27	2.05		3	1.45		
28	5.35		4	1.50		
29	2.40		5	1.50		
30	4.00		6	1.10		
31	2.30		7	1.40		
Subtotal	73.45		8	1.10		
	(August)		9	1.45		
September 1	3.10		10	1.35		
2	6.10		13	2.30		
3	4.10		14	5.50		
4	4.25		19	4.35		
5	0.50		20	1.50		
	Palangka Raya → Banjarmasin (100-hour inspection)		22	2.00		
10	1.50	24	5.00	Demobilization to Jakarta		
12	3.00	Subtotal	37.10	(October)		
13	4.05					

(*) Total survey flight hours from August 7 to October 24

198 hr 20 min

Table 6 List of Survey flight hours (Phase III No. 1, 1977)

Date	Hour	Remarks	Date	Hour	Remarks
March 11	2.00	Test flight at Jakarta	April 29	0.40	Palangka Raya → Banjarmasin (100-hour inspection)
15	3.00	Test flight at Jakarta			
18	5.00	Mobilization to Palangka Raya			
21	0.40	Survey flight start			
22	1.40				
23	1.45				
25	1.50				
30	1.00				
31	2.05				
Subtotal 19.05		(March)	Subtotal 64.10		(April)
April 1	3.10		May 3	1.50	Flight test at Banjarmasin
2	3.10		4	0.55	Banjarmasin → Palangka Raya
3	1.30		5	2.40	
9	1.40		6	3.20	
11	3.25		8	3.15	
"	1.10		10	1.30	
12	4.45		11	4.50	
14	2.00		"	0.45	
16	2.00		12	3.25	
17	1.35		"	0.45	
"	2.30		13	1.50	
18	3.00		"	0.45	
19	2.00		14	5.25	
"	3.00		"	0.50	
21	3.00		15	0.55	
"	3.10		16	5.00	
22	3.50		17	2.20	
23	2.35		"	4.10	
24	3.30		18	1.45	
25	2.45		19	3.35	
26	2.35		20	4.30	
"	3.30		21	3.10	
27	3.40		22	2.00	
			"	3.45	
			23	4.20	
			"	3.20	
			24	2.50	
			"	2.40	
			25	2.25	
			26	3.30	
			Subtotal 82.20		(May)

(* Total Survey flight hours from March 11 to May 26

165 hr 35 min

Table 7 List of survey flight hours (Phase III No. 2, 1977)

Date	Hour	Remarks	Date	Hour	Remarks	
May 27	5.50	Palangka Raya → Banjarmasin (100-hour inspection)	June 19	4.45	Palangka Raya → Banjarmasin (100-hour inspection)	
28	6.15		20	5.00		
29	4.00		21	9.10		
30	5.00		22	6.35		
31	0.50		23	8.00		
Subtotal 21.55		(May)	24	8.30		
June 8	2.20	Banjarmasin → Palangka Raya (including flight test at Banjarmasin)	25	8.40		
Subtotal 100.25			(June)	26		6.50
9	5.20		27	7.05		
10	3.45		28	0.50		
11	3.05		Subtotal 2.20		(July)	
14	3.25		July 7	2.20	Banjarmasin → Palangka Raya (including flight test at Banjarmasin)	
15	5.45		Subtotal 2.20		(July)	
16	4.30					
17	1.15					
18	5.35					

(*) Total survey flight hours from May 27 to July 7

124 hr 40 min

Table 8 Aircraft inspection schedule

Aircraft	Inspection	Date	Airport	City
Cessna 402B PK-VCE	100-hour	Jul. 28, 1976	Kemayoran	Jakarta
	50-hour		Panarung	Palangka Raya
	100-hour	Sept. 5, 1976	Samsudin Nur	Banjarmasin
	50-hour		Panarung	Palangka Raya
	100-hour	Nov. 1, 1976	Kemayoran	Jakarta
Cessna 402B PK-VCD	50-hour	Apr. 21, 1977	Panarung	Palangka Raya
	100-hour	Apr. 30, 1977	Samsudin Nur	Banjarmasin
	50-hour	May 15, 1977	Panarung	Palangka Raya
	100-hour	Jun. 2, 1977	Samsudin Nur	Banjarmasin
	50-hour	Jun. 21, 1977	Panarung	Palangka Raya
	100-hour	Jun. 29, 1977	Samsudin Nur	Banjarmasin

- 4) The final flight path recovery map was completed from the compilation of plotted flight path data on topographic maps and LANDSAT and SLAR imagery photomosaics. Making reference to this map, the following flight schedule and the need for additional survey lines were reviewed.
- 5) The standard magnetic value at the base station was determined as 42,250 gammas. The correction table of daily magnetic variations was made on the basis of the analogue record of time variations from the standard magnetic value. The airborne magnetic data was corrected in reference to the correction table, and thus the local magnetic value, independent of the diurnal effect of the earth's magnetic field, was obtained.
- 6) After correction of daily magnetic variations, the magnetic data by flight was transcribed into the flight path map at every 25 gammas in accordance with the fiducial counts, and the preliminary total magnetic intensity map was prepared.

3-6-2 Data processing

1) Digitization of data

The analogue magnetic data and the flight path recovery data from the field survey were digitized by the use of a Bendix Data Grid Digitizer in Japan.

The flight path data was digitized in the form of the X-Y rectangular coordinates in accordance with 10-second fiducial counts. The analogue magnetic data was digitized from the airborne magnetic recordings at every 10 seconds with the

fiducial counts.

The digitized magnetic data was recorded into magnetic tape and data cards to produce the flight path map and total magnetic intensity map through a CDC 6600 Computer System.

2) Digitization of magnetic data on a square grid

The digitized magnetic data at a 10-second interval was interpolated on a square grid at intervals of 2.5 km (1 cm grid). The origin of the coordinate axis of a square grid is situated at latitude $0^{\circ}00'$, longitude $111^{\circ}45'$.

3) Total magnetic intensity map

The digitized flight path and magnetic data were processed through a computer program, and 10-gamma magnetic intercepts together with anomaly maxima and minima were plotted automatically on the flight path to produce countour map. Checking with the map, it was sometimes found that some differences between magnetic values occur at intersections of traverse and tie lines. These are caused by errors due to positioning, flight altitude and heading of aircraft (heading error is a magnetic change induced by change in flight direction). In case that any magnetic closing error was found at an intersection of traverse and tie lines, the re-examination of positioning and horizontality of the aircraft was made. The closing errors were minimized in a least squares sense by an computer by estimating coefficients of the 1st order trend of closing error for each flight line

to provide final corrections to magnetic values obtained at all intersections. Finally the total magnetic intensity map was drawn on the basis of the data given at the grid points.

4) Residual map

The total magnetic field measured in the direction of the geomagnetic field contains the combined effect of all the magnetic sources present at and below the earth's surface. The shallow crustal bodies normally produce high intensity anomalies of relatively small horizontal extent. On the other hand, the deepseated sources in the interior of the earth generally produce anomalies of vast horizontal extent because of their great depths and sometimes because of their large dimensions. These anomalies are normally characterized by broad and smooth variations over relatively small areas. In such cases, it is highly possible to represent them to a reasonably satisfactory degree in a form of two-dimensional quadratic surfaces fitted to the total field values by the principle of least squares. An undesirable effects of these anomalies distort local anomalies and also tend to mask anomalies due to weak but shallow sources. After removal of these effects, the remaining total field is called the residual.

The residual map was drawn on the basis of the geomagnetic regional variation, which was calculated by subtracting the standard total magnetic intensity of the International Geomagnetic Reference Field (IGRF) from the total magnetic

intensity interpolated on the grid points.

A computer program is provided for the IGRF with position, latitude and longitude, flight elevation of survey and date.

Table 9 summarizes the computations made at 91 points in the survey area at intervals of 10' latitude and 15' longitude.

3-7 Method of analysis

In the airborne magnetic data analysis, there are two different ways of approach; qualitative and quantitative analyses methods. The former is a qualitative speculation of geological features selectively extracted from geomagnetic residual anomalies by means of some filtering procedures. The filters generally used are given as follows :

- a. Second vertical derivative filter
- b. Band-pass filter
- c. Strike filter
- d. Magnetic pole reduction filter
- e. Continuation filter
- f. Auto-correlation analysis
- g. Spectral analysis

etc.

On the other hand, the latter analysis aims at estimating depths, shapes and magnetic properties of rock bodies inducing magnetic anomalies. The corresponding methods are as follows:

- a. Specific point method
- b. Curve matching method

Table 9 IGRF geomagnetic component in central Kalimantan (1977.5)

Longitude (E) Latitude (S)	111°45'	112°00'	112°15'	112°30'	112°45'	113°00'	113°15'	113°30'	113°45'	114°00'	114°15'	114°30'	114°45'
0°00'	41662.3	41646.2	41629.8	41613.5	41596.8	41579.9	41562.9	41545.8	41528.4	41510.9	41493.3	41475.5	41457.5
0°10'	41713.3	41697.2	41680.9	41664.6	41647.9	41631.1	41614.3	41597.2	41580.0	41562.6	41545.0	41527.3	41509.4
0°20'	41764.7	41748.7	41732.6	41716.3	41699.7	41683.0	41666.3	41649.2	41632.1	41614.8	41597.3	41579.8	41562.0
0°30'	41817.0	41801.2	41785.1	41768.9	41752.5	41735.8	41719.2	41702.3	41685.2	41668.0	41650.6	41633.1	41615.4
0°40'	41870.6	41854.8	41838.8	41822.7	41806.3	41789.9	41773.2	41756.4	41739.5	41722.4	41705.1	41687.9	41670.3
0°50'	41925.0	41909.3	41893.4	41877.4	41861.1	41844.8	41828.3	41811.6	41794.6	41777.6	41760.6	41742.9	41725.5
1°00'	41979.9	41964.3	41948.5	41932.6	41916.4	41900.2	41883.6	41867.0	41850.3	41833.5	41816.7	41799.0	41781.8

c. Specific curve method

d. Analytical method

etc.

A flow chart of data processing and analysis is shown in Fig. 7.

3-7-1 Spectral analysis

An aeromagnetic map usually contains a number of features which are superposed on each other. These features may be composed of regional, local and microanomalies. The aim of an interpretation of such maps is to extract as much useful information as possible from the data. Since one type of anomaly often masks another one, there is a need to separate various features from each other.

The anomalies produced by shallow bodies are normally characterized by their sharpness and high intensity. They are small-wavelength anomalies in the magnetic map. On the other hand, the deep-seated magnetized masses give rise to large-wavelength, low-intensity anomalies. It is, therefore, recognized that under suitable conditions a deep causative body can be represented in its own band of wavelength different from that of shallow bodies. This fact provides the foundation for the application of frequency filtering techniques to the relative emphasis and de-emphasis of certain features in the magnetic data.

The characteristics of wave length of magnetic anomalies are usefully applied to a magnetic analysis through data processing as well as to an estimate of mean depth of magnetic basement by using the potential theory.

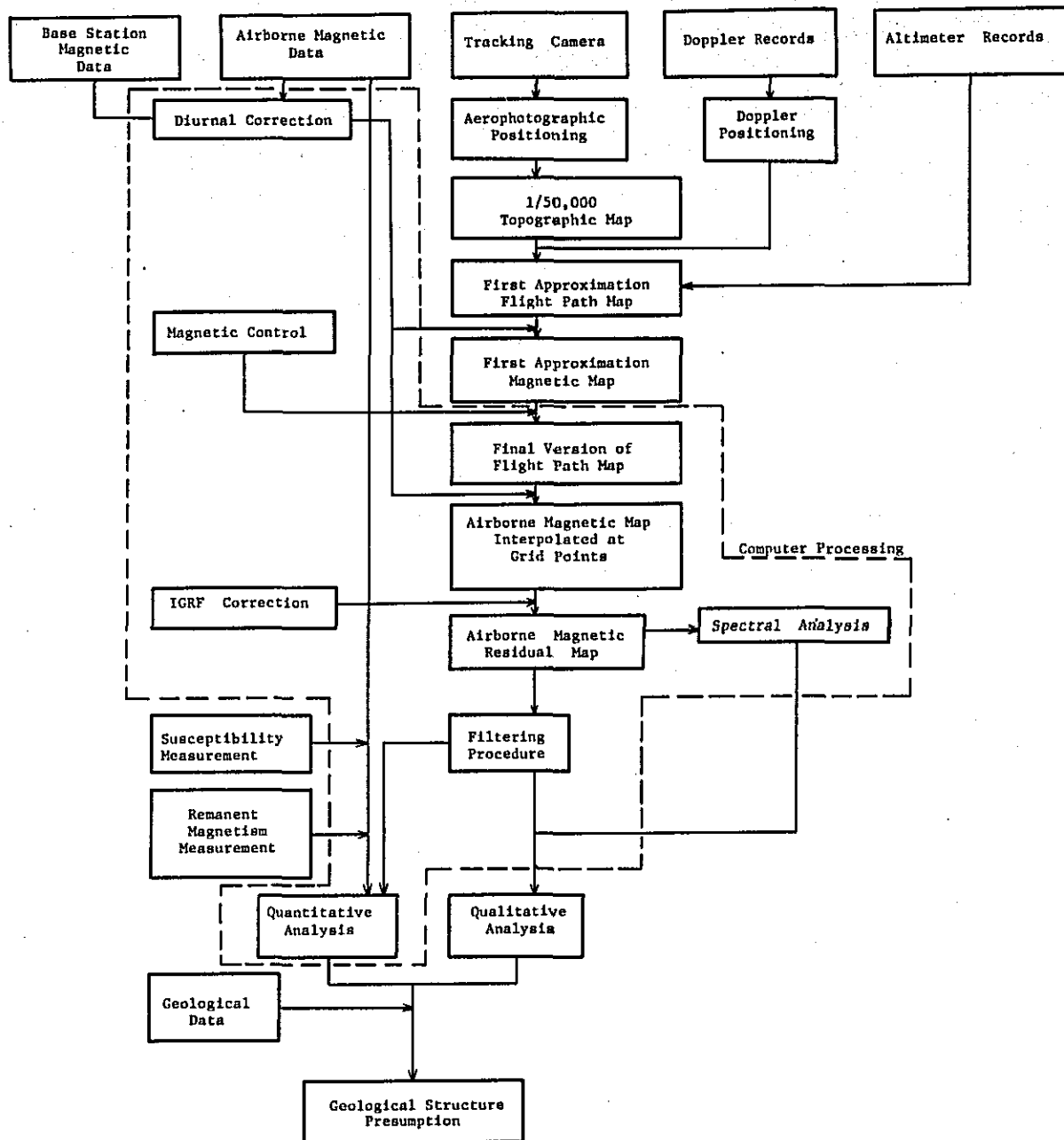


Fig. 7 Flow chart of data processing and analysis

a. Energy spectrum

An observed value $F(x,y)$ in the rectangular coordinates is expressed in a two-dimensional Fourier series as

$$\begin{aligned}
 F(x,y) = & \sum_{m=0}^M \sum_{n=0}^N (A_{mn} \cos \frac{2m\pi x}{L_1} \cos \frac{2n\pi y}{L_2} \\
 & + B_{mn} \cos \frac{2m\pi x}{L_1} \sin \frac{2n\pi y}{L_2} + C_{mn} \sin \frac{2m\pi x}{L_1} \cos \frac{2n\pi y}{L_2} \\
 & + D_{mn} \sin \frac{2m\pi x}{L_1} \sin \frac{2n\pi y}{L_2} \quad (1)
 \end{aligned}$$

Hence, the Fourier coefficient A_{mn} is given by

$$A_{mn} = \frac{4}{L_1 L_2} \int_0^{L_1} \int_0^{L_2} F(x,y) \cos \frac{2m\pi x}{L_1} \cos \frac{2n\pi y}{L_2} dx dy \quad (2)$$

where the data of F are uniformly distributed over an area of $L_1 \times L_2$. Similarly, we can obtain B_{mn} , C_{mn} and D_{mn} .

For a computer use, the data of F are given on a rectangular grid with spacings of Δx and Δy ; i.e. $F(i,j)$ at the (i,j) th grid point by defining $x = i\Delta x$ and $y = j\Delta y$. Then, Eq.(2) can be rewritten in the form:

$$\begin{aligned}
 A_{mn} = & \frac{4}{L_1 L_2} \Delta x \Delta y \sum_{i=0}^{L_1/\Delta x} \sum_{j=0}^{L_2/\Delta y} W_{ij} F(i,j) \cos \frac{2m\pi i \Delta x}{L_1} \\
 & \cos \frac{2n\pi j \Delta y}{L_2} \quad (3)
 \end{aligned}$$

where W_{ij} is the weight function in the two-dimensional trapezoidal rule of numerical integration.

The energy spectrum is then obtained as

$$E_{mn} = A_{mn}^2 + B_{mn}^2 + C_{mn}^2 + D_{mn}^2$$

b. Estimation of mean depth to magnetic basement

Suppose that an energy spectrum of magnetic anomalies due to a magnetic layer lying at a depth of H is "white".

The potential theory leads the following relation between the energy spectrum E_{mn} of wave numbers (m,n) and H. It is

$$E_{mn} \propto e^{-4\pi HF} \quad (4)$$

where f is a quantity called frequency :

$$f = \sqrt{\left(\frac{m}{L_1}\right)^2 + \left(\frac{n}{L_2}\right)^2}$$

The energy spectrum is plotted in an f vs. $\log E_{mn}$ graph. A straight line is determined by the least square fitting to the plots. Taking Eq. (4) into consideration, H can be estimated from the tangent of the straight line.

3-7-2 Second vertical derivative filter

The second vertical derivative method is based on the relative emphasis of local anomalies and de-emphasis of regional anomalies. The second vertical derivative is a negative of the sum of two horizontal second derivatives. Hence it is a measure of changes in the magnetic gradient and then derivative anomalies are coincident with the nonlinear part of the observed total magnetic intensity map. Another interesting feature of the derivative map is that it tends to delineate magnetized geological formations. The zero contour of the map is very effective in outlining the horizontal boundaries of the causative bodies.

The computation of second vertical derivative is made on the basis of the formulas by Rosenbach, and Henderson and Zietz for the peripheral data.

The formulas are given by :

$$\frac{\partial^2 \Delta T}{\partial Z^2} = \frac{1}{S^2} \frac{1}{24} (96 \Delta T_0 - 72 \Delta T_1 - 32 \Delta T_2 + 8 \Delta T_4) \quad (\text{Rosenbach})$$

$$\frac{\partial^2 \Delta T}{\partial Z^2} = \frac{2}{S^2} (3 \Delta T_0 - 4 \Delta T_1 + \Delta T_2) \quad (\text{Henderson and Zietz})$$

where,

$$\Delta T_1 = \frac{\Delta T_{11} + \Delta T_{12} + \Delta T_{13} + \Delta T_{14}}{4}, \quad \Delta T_2 = \frac{\Delta T_{21} + \Delta T_{22} + \Delta T_{24}}{4}$$

$$\Delta T_4 = \frac{\Delta T_{41} + \Delta T_{42} + \Delta T_{43} + \Delta T_{44} + \Delta T_{45} + \Delta T_{46} + \Delta T_{47} + \Delta T_{48}}{8}$$

The configuration of T_{11} , T_{12} , , T_{48} are shown in Fig. 8.

3-7-3 Magnetic pole reduction filter

The geomagnetic vector at a site of observation and a magnetization vector associated with the causative body are important parameters in determining the size and shape of an anomaly. For reliability and accuracy in magnetic interpretation it would be desirable to evaluate a hypothetical anomaly from the observed anomaly on the assumption that the causative body is physically moved to the north pole and the magnetization vector becomes vertical by transformation. Such a hypothetical anomaly can be evaluated in a form of the two-dimensional harmonic expansion of the total field values. The resulting anomaly thus obtained apparently looks like a gravity anomaly.

For reduction of the total field to the pole, the magnetization is assumed to be induced alone by rock masses because the actual magnetization vector is unknown. In some cases such an assumption may lead to erroneous results. In most cases, however,

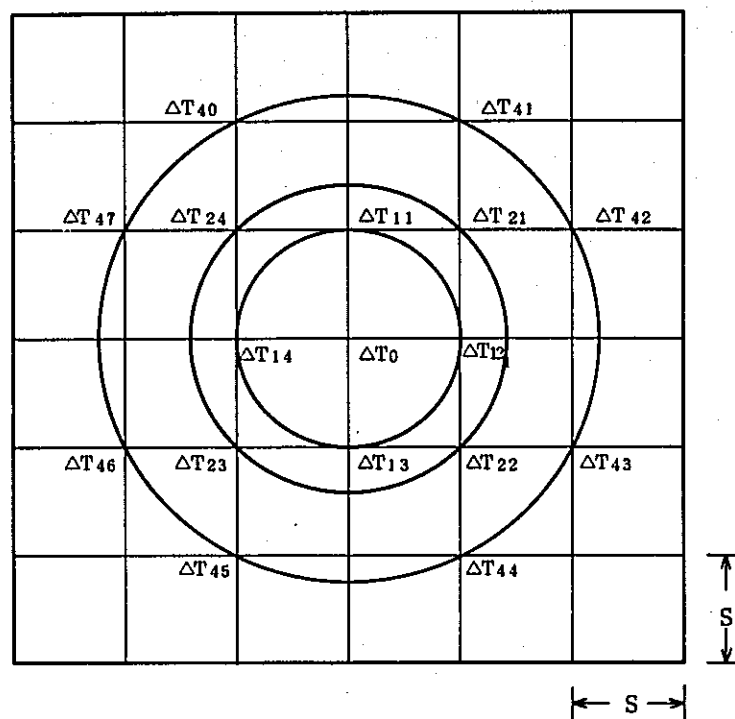


Fig. 8 Lattice configuration for second vertical derivative calculation

the reduced maps give us more consistent results than the original maps.

In a practical computation, $T(x,y)$, the anomaly values of the total magnetic intensity are read at a grid point with an interval of S in the rectangular coordinates, where the direction of the magnetic north is adopted as the y -axis. Based on the regional tendency $N(x,y)$, calculated by the least squares method from the $T(x,y)$, the residual values at grid points are obtained as

$$\Delta TR(x,y) = T(x,y) - N(x,y)$$

The values at rectangular grid points are finally calculated by taking convolution products of $\Delta TR(x,y)$ with weights defined as

$$W^{-1}(x', y') = \frac{1}{2\pi^2 sa} \int_{\frac{1}{N}}^1 \int_{\frac{1}{N}}^1 e^{2\pi h' \sqrt{m^2 + n^2}} - \frac{1}{\sqrt{m^2 + n^2}} \cos 2\pi(mx' + ny') dmdn$$

The lattice configuration for the calculation of magnetic pole reduction is shown in Fig. 9.

3-7-4 Quantitative analysis

An automatic interpretation of the total magnetic intensity due to two-dimensional bodies is a very useful method to determine the depth, position and magnetization of a set of uniformly magnetized bodies consisting of faults or dikes or their combinations from an anomaly profile. The method employs a non-linear transformation which makes it possible to replace a non-linear process in the interpretation with a series of linear processes. The outline of this method is described as follows.

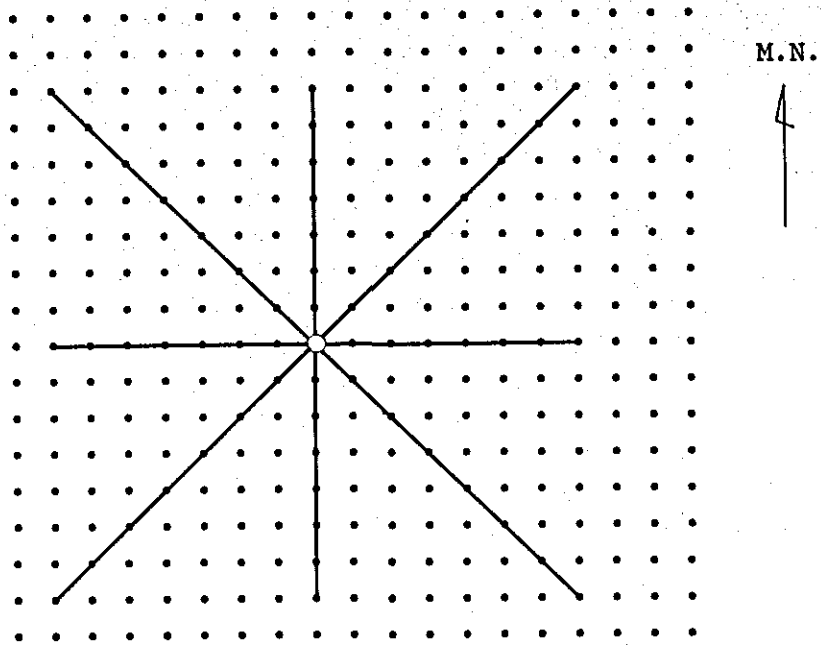


Fig. 9 Lattice configuration for magnetic pole reduction calculation

When $F(\omega)$ is the Fourier transform defined by the formula

$$T(x) = \sum_{m=0}^M A_m e^{-j2\pi mx} \quad (1)$$

for a magnetic profile $T(x)$, and this mutual relation is represented by :

$$T(x) \leftrightarrow F(\omega) = A_m(\omega) + j B_m(\omega) \quad (2)$$

where, $\omega = 2\pi m$ and $j = \sqrt{-1}$

the horizontal derivative $T_x(x)$ and the vertical derivative $T_z(x)$ is given by :

$$T_x(x) = \frac{\partial T(x)}{\partial x} \leftrightarrow j\omega F(\omega) = -\omega B(\omega) + j\omega A(\omega) \quad (3)$$

$$T_z(x) = \frac{\partial T(x)}{\partial z} \leftrightarrow \omega F(\omega) = \omega A(\omega) + j\omega B(\omega) \quad (4)$$

The derivative operation becomes very simple in the frequency domain and it makes easy to get the higher derivatives.

We then introduce a Bell type function $a(x)$ defined by :

$$a(x) = (T_{xz}(x))^2 + (T_{zz}(x))^2 \quad (5)$$

For a two-dimensional model, such as a fault or dyke-like structure, $a(x)$ becomes simple expressions as follows.

$$\text{Fault structure : } a_F = \beta^2 [(x - x_0)^2 + h^2]^{-1} \quad (6)$$

Dyke structure :

$$a_D = 4\beta^2 d^2 [(x - x_0 - d)^2 + h^2]^{-1} \cdot [(x - x_0 + d)^2 + h^2]^{-1} \quad (7)$$

where,

$$\beta = kT_0 \cdot (1 - \cos^2 i \cdot \sin^2 \alpha)$$

k = susceptibility contrast

T_0 = total magnetic field

i = average inclination

α = angle between the magnetic north and magnetic profile

x_0 = position of model structure

$2d$ = width of a dyke body

h = depth of the top of a body

The procedure of computation is described as follows.

A fast digital Fourier transform technique is applied to each magnetic profile to get complex frequency domain values. After the second derivative operations, the data is re-transformed back to spacial domain by the reverse Fourier transform. Then the Bell type function $a(x)$, a curve matching process with least squares method is applied to decide the type of structure for regions near the maximum value point. Then, the apparent susceptibility, depth and width can be determined automatically.

3-8 Measurement of rock magnetism

The susceptibility measurements were made on 23 samples, collected from the geological surveys, at the Geological Survey of Indonesia by means of a Bison Susceptibility Meter. The results of these measurements are listed in Table 10.

The mean values of magnetic susceptibility amount to

$3,992 \times 10^{-6}$	cgsemu/cc for 3 Andesite samples
$1,479 \times 10^{-6}$	cgsemu/cc for 3 Dioritic rock samples
120×10^{-6}	cgsemu/cc for 8 Sandstone samples
48×10^{-6}	cgsemu/cc for 2 Limestone samples
64×10^{-6}	cgsemu/cc for 3 Shale samples
99×10^{-6}	cgsemu/cc for 2 Slate samples
99×10^{-6}	cgsemu/cc for 2 Schist samples

Table 10 Susceptibilities of rock samples

Sample No.	Rock name	Susceptibility $\times 10^{-6}$ cgsemu/cc	Mean susceptibility $\times 10^{-6}$ cgsemu/cc
OK- 7	Andesite	3307	3992
OK- 112	Andesite	4574	
TS-1670	Andesite	4096	
TS- 462	Dioritic rock	963	1479
TS- 340	Dioritic rock	2211	
VE- 5	Dioritic rock	1264	
OK- 336	Sandstone	351	120
OK- 36	Sandstone	46	
OK- 43	Sandstone	15	
TS- 707	Sandstone	75	
TS- 850	Sandstone	35	
TS- 925	Sandstone	369	
OK- 213	Sandstone	15	
OK- 219	Sandstone	57	
OK- 68	Limestone	53	48
OK- 130	Limestone	42	
OK- 392	Shale	60	64
OK- 72	Shale	53	
OK- 126	Shale	80	
TS- 558	Slate	29	99
TS-3682	Slate	169	
TS-1258	Schist	186	99
OK- 247	Schist	11	

Chapter 4 Survey Results

The survey results are illustrated in six kinds of magnetic maps: residual map, second-vertical derivative maps, magnetic pole reduction map, deep and shallow effects maps of spectral analyses (see PL. I - VI). Interpretation map (PL. VII) summarizes the results of qualitative and quantitative analyses of the obtained magnetic anomalies, magnetic measurements of rock samples and the available geological data.

4-1 Residual map (PL. I)

The magnetic feature of the survey area, quantitatively extracted from the residual anomaly pattern in the residual map, is as follows.

Judging from the magnetic feature, the survey area can be divided into three parts : the Northwestern, the Southwestern and the Eastern Parts, which are respectively denoted by Areas I, II and III (see Fig. 10).

Area I : This area is predominantly occupied by very weak magnetic anomalies of long wavelength amounting to about 40 - 60 km with the amplitude of 50 - 60 gammas. From the magnetic feature, Area I is subdivided into three sections : ① a large-scale magnetic structural line expressed by magnetic contours extending in a WNW-ESE direction from the northwestern to the southeastern parts of Area I. ② Magnetic structural line trending NNE-SSW cross the northern borderline of Area I. And ③ A large-scale magnetic basin-like structure consisting of gently-sloped anomalies of very

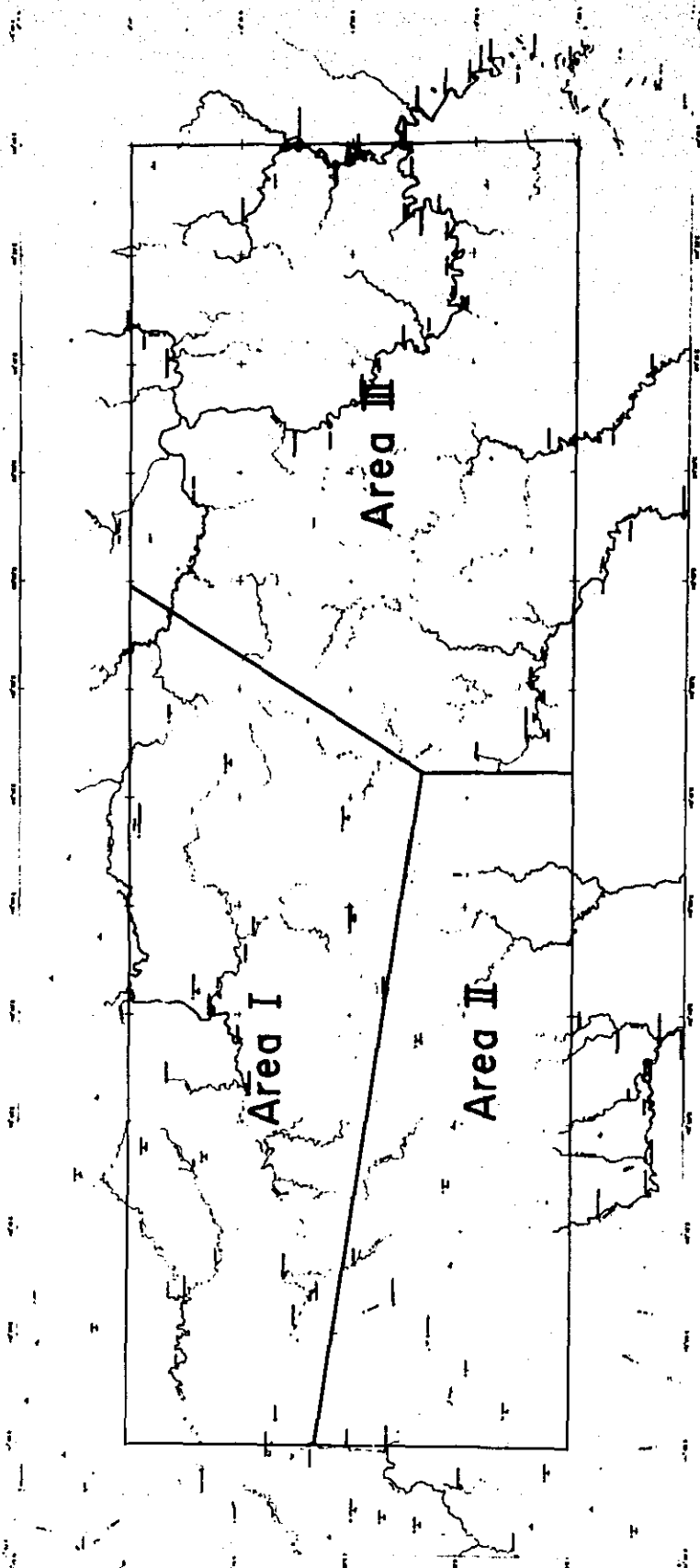


Fig. 10 Sectional map of survey area

long wavelength, which stretches extensively over the eastern part of Area I.

Area II : This area is characterized by the local concentration of sharp magnetic anomalies of short and medium wavelength about 10 - 30 km long with the amplitude of 100 - 700 gammas. The significant magnetic feature there is as follows. ① Relatively large-scale anomalies of medium wavelength extended in a direction of WNW-ESE or E-W. ② NW-SE or WNW-ESE trending magnetic structural lines accompanying the anomalies as mentioned above. ③ Short wavelength anomalies predominantly stretching in a ENE-WSW or NE-SW direction. And ④ NE-SW trending magnetic structural lines accompanying the above-mentioned anomalies.

Area III : This area consists of magnetic anomalies having both the characteristic features of Areas I and II. That is to say, relatively gently-sloped magnetic anomalies are found along the northern and eastern borderlines of this area, but the remaining parts are occupied by sharp anomalies of short and medium wavelength. The significant magnetic feature reflecting the geological structure is as follows. ① Magnetic structure corresponding to the relatively gently-sloping anomalies found along the northern and eastern borderlines of this area. ② WNW-ESE trending anomalies found in the central part of the northern borderline. ③ NS trending anomalies in the southwestern part of this area. ④ Complicated structure expressed by a cluster of anomalies arranging along E-W or NE-SW directions in the central part of this area ⑤ E-W trending

structure corresponding to relatively sharp magnetic anomalies distributed over the southern part of this area. ⑥ A large-scale NE-SW trending magnetic structural line extracted from the systematic distortion of magnetic contours which is recognized in the central part. And ⑦ another large-scale magnetic structural line corresponding to very sharp anomalies having a NE-SW trend in the central part of this area.

4-2 Second vertical derivative map

The second vertical derivative maps are based on numerical filtering calculation results with grid intervals of 1 cm (Second vertical derivative map-1) and 3 cm (Second vertical derivative map-2).

1) Second vertical derivative map-1 (PL. II)

This map shows explicitly the magnetic structural lines by disclosing boundaries between highly-magnetized sources and the adjacent rocks.

Area I : This area is characterized by low-magnetized rocks except relatively high magnetization seen in the central northern, the central eastern and the southern ends. The magnetic anomaly of the southern end has a tendency to decrease northwards. This fact may indicate the related magnetic source is inclined northwards from the northern part of Area II to the southern end of Area I. The magnetic structural lines run in the directions of NE-SW and NW-SE, which may reflect faulting zones or boundaries of rocks.

Area II : This area is predominantly occupied by conspicuous swarm of magnetic anomalies, which are classified into three grades : magnetic high, medium and low. The magnetic highs are located in the northern, the southwestern, the central southern and the eastern parts of this area. The magnetic mediums are found in the western and eastern parts, and lows is widely extended in the central part. The rather small-scale anomalies are also recognized in the northwestern and eastern parts. In the northern, western and eastern parts, many prominent magnetic structural lines run predominantly in the direction of NE-SW, but partially in the directions of NW-SE, WNW-ESE and ENE-WSW. The E-W trending arrangement of magnetic sources is cut by these magnetic structural lines in some places. The general geological feature of this area is represented by the WNW-ESE trending somewhat large-scale magnetic structural line together with the E-W trending one.

Area III : There are three outstanding magnetic anomalies III-①, III-⑤ and III-⑥ in Area III. These may be caused by the extremely high magnetization. The magnetic anomaly swarms are extending from the central western end in the direction of E-W, from the eastern end to the southwestern end in the direction of ENE-WSW, from the central northern end in the direction of WNW-ESE, and from the central eastern end in the direction of NE-SW. The other swarm is also located east of the southern end. These may be due to buried highly-magnetized sources.

2) Second vertical derivative map-2 (PL. III)

In this map a very weakly-magnetized structure is seen, extended

from north of Area I to northwest of Area III in the direction of E-W. Furthermore, a NW-SE trend of magnetization from west of Area II to its central part, and a ENE-WSW trend from east of Area II and west of Area III to its central part are seen in the map. Another trend of NE-SW is also seen in the eastern part of Area III. The grid used here for numerical calculations has three times larger interval than the one used for map-1, so that the sources corresponding to these magnetic anomalies must be comparatively larger in scale.

4-3 Magnetic pole deduction map (PL. IV)

There are marked magnetic highs in the southwestern and eastern ends of Area II and in the central and eastern parts of Area III. These highs may be presumably caused by highly-magnetized rocks widely lying in these areas. The east side of the central part of Area III is occupied by gently-sloped anomalies, on the other hand, the west side by complex short-wavelength magnetic anomaly swarms. This may indicate that both the sides have different geology each other, and perhaps that the magnetic sources are deepseated in the east side, on the other hand, shallowseated in the west side.

4-4 Spectral analysis map

Fig. 11 shows a relation between energy spectrum and frequency of magnetic anomalies on the basis of the residual map. As seen in this figure, the spectrum distribution is divided into two parts at a frequency of 0.06 cycles/km (wavelength of about 17 km). The

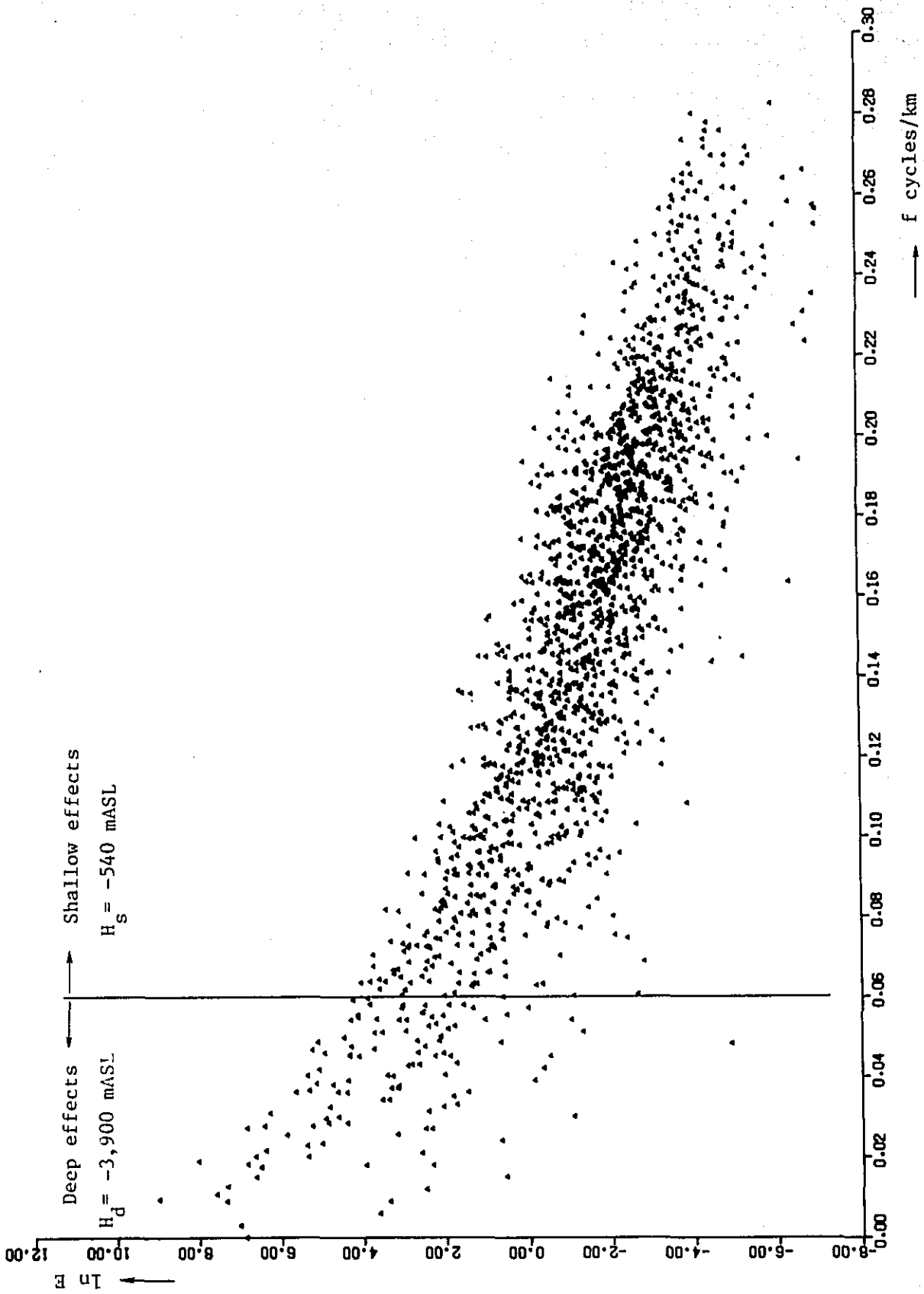


Fig. 11 Energy spectrum vs. frequency

lower frequency part is thought to be a response of the deep magnetic structure, on the other hand, the higher part may presumably reflect the shallow one. Straight lines are fitted to the frequency distribution by the least squares method to obtain the gradients of the straight lines. As a result, the mean depths of the shallow and deep structures are calculated as .540 m and 3,900 m below sea-level, respectively. The maps of deep and shallow effects are drawn on the basis of the results thus calculated.

1) Spectral analysis map - Deep effects (PL. V)

This map reflects magnetic effects of deep and large-scale structure, i.e. spatial distribution of deepseated magnetic bodies. In Area I, the deep effects express the existence of weakly magnetized bodies, which, as a whole, are lining up in the direction of E-W, with the exception of WNW-ESE trending in the west and ENE-WSW in the east. In Area II, strongly magnetized bodies are distributed in the direction of WNW-ESE. At the northwestern, the northeastern and the central eastern corners of Area III, the weakly magnetized bodies are recognized. But the remaining parts are predominantly occupied by highly-magnetized ones, which trend in the direction of E-W or ENE-WSW in the west central and the southern parts of this area, and in the direction of NW-SE in the northern part.

2) Spectral analysis map - Shallow effects (PL. VI)

This map expresses selectively the magnetic effects of near-surface and shallowseated rocks. Through the northern part of Area I and the northwestern part of Area III, the E-W trend of weak

magnetization is seen. In the southern part of Area I, there is a relatively strong magnetization zone running in the direction of WNW-ESE. Area II, as a whole, is occupied by highly-magnetized bodies, which are recognized especially in the western, the central northern, the central southern and the eastern corners of this area. In Area III, highly-magnetized bodies are extensively distributed in the NE-SW trend over the central western part, the central northern corner and the central eastern parts of this area.

4-5 Quantitative analysis

Quantitative computer analyses are applied to the magnetic anomaly profiles on the basis of the residual map. For the computer results, propriety is to be tested and verified in width, depth and apparent susceptibility of magnetic source. Taking into consideration of the geological data, model analyses are done by the use of Talwani method to obtain the most consistent models with geology. These computed results are shown in Table 11. The results of the analyses are summarized as the interpretation map in PL. VII.

Table 11 Results of qualitative analysis

Anomaly No	Profile No	Automatic analysis			Talwani method		
		Width (m)	Depth (mASL)	Susceptibility ($\times 10^{-3}$ gsemu/cc)	Width (m)	Depth (mASL) Top/Bottom	Susceptibility ($\times 10^{-3}$ gsemu/cc)
I - ①	I - ① - 1	2,650 0	- 1,750	0.5	2,650 0	- 3750/-∞	1.1
II - ①	II - ① - 1	1,000 0	- 750	1.3	7,500	+ 500/-∞	3.6
	II - ① - 2	1,050 0	0	2.1	7,300, 5,200	+500/-∞, +500/-1750	2.7
II - ②	II - ② - 1	4,000 0	+ 1,250	1.8	5,500 0	+1250/-∞	1.9
	II - ② - 2	3,500 0	+ 1,250	1.0	2,700	+1000/-∞	1.3
II - ③	II - ③ - 1	1,650 0	- 750	1.8	13,000, 4,000	+1500/-1750, +1250/-∞	1.4
	II - ③ - 2	1,250 0	- 1,250	3.1	5,000, 7,300	+500/-∞, +500/-3000	2.0
II - ④	II - ④ - 1	5,500 0	- 1,000	2.7	9,400	+ 250/-∞	2.0
	II - ④ - 2	7,000 0	0	2.5	5,000, 3,700	+250/-1750, +250	2.5
II - ⑤	II - ⑤ - 1	—	—	—	8,800, 6,200 3,000	+500/-1250, +500/-∞, +500/-2000	4.1
	II - ⑤ - 2	—	—	—	5,000 0	+1000/-∞	1.3
II - ⑥	II - ⑥ - 1	8,500 0	- 2,750	4.5	8,700, 3,600	0/-∞, 0/-2250	1.2
	II - ⑥ - 2	7,000 0	+ 250	5.1	5,000 0	+ 250/-∞	2.2
III - ①	III - ① - 1	—	—	—	6,700, 13,300	+1000/-1500, +1000/-∞	1.5
	III - ① - 2	8,000 0	- 1,250	3.9	8,800 0	+ 250/-∞	1.4
III - ②	III - ② - 1	—	—	—	5,800 0	- 250/-∞	1.5
	III - ② - 2	—	—	—	2,250 0	- 2750/-∞	1.6
III - ③	III - ③ - 1	—	—	—	6,700, 4,600 3,400	+250/-750, +250/-3000, +250/-500	3.9
	III - ③ - 2	—	—	—	8,800 0	+750/-2000	4.1
III - ④	III - ④ - 1	—	—	—	6,200 0	+1000/0	3.6
	III - ④ - 2	—	—	—	5,200 0	+250/-500	4.3
III - ⑤	III - ⑤ - 1	—	—	—	6,700, 6,700 3,600	-250/-1500, -250/-4750, -250/-1500	4.2
	III - ⑤ - 2	—	—	—	6,600 0	+ 250/-250	3.6

Chapter 5 Summary of Results

Judging from the obtained magnetic feature, the survey area is divided into three parts : the northwestern part (Area I), the southwestern part (Area II) and the eastern part (Area III).

Area I is characterized by very low magnetic anomalies of long wavelength in contrast to Area II occupied by a swarm of extremely high magnetic anomalies of short or medium wavelength. Area III has a mixed characteristic feature of the above two areas.

Results of magnetic measurement of rock samples indicate the facts that andesite and dioritic rock show very large susceptibilities but sandstone, limestone, shale, slate and schist show very small ones. It is concluded on the basis of these facts that the extremely high magnetic anomalies may be caused by andesite and dioritic rock, on the other hand, the low anomalies may attribute to the other sedimentary rocks.

In view of these facts, it is presumed that the sedimentary rocks may cover Area I and the especially thick layers may form the large-scale magnetic basin-like structure in the eastern part of Area I. As a matter of fact, geological data available for this part support the wide distribution of sandstone, mudstone and shale. Although rock magnetism has never tested for mudstone samples, they are expected to show low susceptibility of the same order as sandstone. In conclusion, Area I is occupied by thick layers of sandstone, mudstone and shale, and the maximum thickness of the layers amounts

to 4,000 m deep below sealevel as indicated by the deep effects obtained from the spectral analyses of the magnetic data with respect to the large-scale magnetic basin-like structure.

The extremely high magnetic anomalies extensively distributed over Area II may be caused by highly-magnetized rocks such as andesite and dioritic rock. It is also expected from the geological standpoints that shale, slate, schist, gneiss together with granitic rock are distributed over this area. The results of analysis indicate the magnetic anomalies there are classified into three kinds on their magnitude : high, medium and low.

The highs (II-①, II-②, II-③, II-④, II-⑤, II-⑥, etc.) correspond to the distribution of granitic rock partially assorted with gneiss, slate or schist as directly proved on the geological data. It is highly possible that these magnetic highs may correspond to dioritic rock or granitic rock with basic composition.

The medium magnetic anomalies in Area II well coincide with the granitic rock distribution as compared with the geological data. Although rock magnetism has never tested for granite specimens, it is generally true that granite indicates susceptibility lower than dioritic rock. Taking these facts into consideration, the medium anomalies may be possibly caused by granite or somewhat-dioritic granite.

Meanwhile, the magnetic lows in Area II correspond to weakly-magnetized granitic rock assorted with schist or slate.

In Area III, three conspicuous magnetic anomalies (III-①, III-⑤ and III-⑥) are recognized, which have magnetic patterns similar to some of the highs obtained in Area II.

On the analogy of the magnetic patterns, III-⑤ is presumed to be caused by andesite. According to the magnetic analyses, the thickness of the magnetic source is estimated as about 3,000 m.

Many andesite outcrops are found around III-⑥, although its magnetic pattern is apparently similar to that of sandstone, conglomerate and shale distribution in Area II. The magnetic source andesite covers extensively over III-⑥, and its thickness is estimated as about 3,000 m.

Slate, schist and granitic rock are distributed over III-① anomaly, but the result of the magnetic analyses comes to a conclusion that the magnetic source concerned may be shallow-seated dioritic rock having a deep root.

Relatively high anomalies (III-② and III-③) are found east and south of III-①, respectively. The former is located in an area of sandstone, gneiss, slate and schist and the latter in a gneiss and andesite outcropping area dotted with a small-scale granitic outcrops. According to the magnetic analyses, however, the magnetic sources are thought to be highly magnetized dioritic rocks. The depths of the buried sources are estimated as 1,000 m and 250 m ASL, respectively.

There are found small-scale but rather outstanding anomalies

corresponding to andesite and sandstone outcrops in the central and eastern parts of Area III. Andesite forms the sources of these anomalies.

The analytic result indicates that III-④, which is found in the northern central part of this area, is due to the relatively deepseated magnetic source with a depth of -250 m ASL. This anomaly is located in an area of sandstone and partially basement gneiss, so that highly magnetized basement dioritic rock may be possibly distributed as magnetic sources.

III-⑦, which is found in the southeastern corner of Area III covered with sandstone and shale, reflects a highly-magnetized source, which may be possibly buried dioritic rock intrusions penetrating slate and schist as seen north of this anomaly.

In the northeastern and eastern corners of this area, gently-sloped magnetic anomalies are distributed over thick layer of sandstone and shale. The central anomalous zone extends southwestwards and further westwards from the eastern corner of this area. This may indicate thick layers of weakly magnetized rock like sandstone or shale.

Although rock magnetism has never tested for gneiss samples, it is presumed that a possible cause of the gently-sloped magnetic anomalies found in the northwestern part may be the wide distribution of weakly-magnetized gneiss.

Another anomaly III-④ found north of the above anomalies is due to relatively deepseated highly-magnetized dioritic rock, which may be inclined southwards to the bottom of the source of the above-mentioned gently-sloped anomalies.

Comparisons between geological data and the magnetic survey results come to the following conclusions of geological structure in the survey area.

Granitic rock forming the basement structure extends in the direction of WNW-ESE over the whole of Area II. On the analogy of the distribution pattern of the magnetic source, probably dioritic rock, in the southwestern part of Area III, it seems likely that the highly-magnetized basement rocks extend in the direction of ENE-WSW with branches stretching toward the central northern boundary and eastwards up to the southern tip of Area III.

Sedimentary rocks such as sandstone, mudstone, shale, etc. are distributed in the direction of E-W extensively over the whole of Area I. It is also presumed that they form thick layers around the magnetic basin structure obtained in the east of Area II. The thickness may amount to 4,000 - 5,000 m.

The magnetic structural lines which, in general, has relation to faults or lineaments, run in the directions of WNW-ESE, NNE-SSW and NW-SE in Area I. The WNW-ESE magnetic structural line is presumed to reflect the large-scale geological structure controlling the basement rock distribution. There are many conspicuous magnetic

structural lines, running in the directions of WNW-ESE in Area II and NE-SW in Area III, which may also reflect the large-scale geological structures controlling the basement rock distribution. Especially, the structural lines in Area III is well consistent with the faults revealed by the geological surveys. The magnetic structural lines comparatively small with that of the above-mentioned run predominantly in the directions of NE-SW and NW-SE in Area II and NE-SW, NW-SE and ENE-WSW in Area III. These are presumably caused by the highly-magnetized basement rock distribution.

The mineralized zones are found by the geological survey from the eastern end of Area II to the western part of Area III. The corresponding mineralized zones tend to distribute around the magnetic anomalies II-④, III-① and III-③, where full of magnetic structural lines running in the directions of NE-SW, NW-SE and ENE-WSW, the trend of the basement rock structure turning its direction from WNW-ESE to ENE-WSW. From the geology, the mineralization is presumed to have a relation with the Tertiary granite. Although the distribution of the Tertiary granite is not clarified from the present survey, it is probably true that, judging from the above described complex geology, the geological condition of forming the mineralization related Tertiary granite is satisfied there.

Chapter 6 Conclusion

The present work contributes to clarifying the geological structure and the igneous rock distribution in the survey area on the basis of the airborne magnetic survey. Granitic rocks forming the basement structure are extensively distributed over the Southwestern Part of the survey area in the WNW-ESE trend and extend from the Central Part to the central Eastern Part in the ENE-WSW trend. The further extension may presumably cover the northeastern and southeastern borderlines of the Eastern Part.

Sandstone, mudstone, shale, etc. are distributed in the direction of E-W over the Northwestern Part of the survey area. They can form very thick layers in the eastern section of the Northwestern Part. The predominant distribution of andesitic rocks in the central section of Eastern Part.

The magnetic feature well reflects the geological structure running in the WNW-ESE trend in the western part but in the ENE-WSW trend in the eastern part of the survey area. The basement structure is considered to be well consistent with the general tendency of the magnetic feature.

The mineralized zones promising for ore deposits are found in the south of the Central Part by the geological survey. The corresponding mineralization is presumed to have a relation with the Tertiary granite. Although the distribution of the Tertiary granite has not been disclosed by the present survey, it is pointed out that the

Tertiary granitic rocks concentrate around the magnetized bodies in the south of the Central Part. Judging from the survey results that the basement structure turns its trend from WNW-ESE to ENE-WSW and the magnetic evidence of existing a number of fault lines, the south of the Central Part is composed of the complex geology. In such a district, the geological condition of forming the Tertiary granite may be satisfied.

Based on the results mentioned above, for the next-year program of this project, the further geological survey including geochemical prospecting is deeply desired to be concentrated into the south of the Central Part for the purpose of selecting spots promising ore deposits.

REFERENCES

1. Direktorat Geologi Indonesia, 1969, Peta geologi, Kalimantan Tenggara, skala 1 : 500,000.
2. Direktorat Geologi Indonesia, 1970, Peta geologi, Kalimantan Barat dan Barat - Daja, skala 1 : 500,000.
3. Edited by Morley, L. W., 1967, Mining and groundwater geophysics : Economic Geology Report, no. 26, Geological Survey of Canada.
4. Spector, A. and Grant, F.S., 1970, Statistical models for interpreting aeromagnetic data : Geophysics, vol. 35, p. 293-302.
5. Henderson, R.C. and Zietz, I., 1949, Computation of second derivative of geomagnetic field : Geophysics, vol. 14, no. 4, p. 508-516.
6. Rosenbach, O., 1953, A contribution to the computation of the "second derivative" from gravity data : Geophysics, vol. 18, no. 4, p. 894-909.
6. Baranov, V., 1957, New method for interpretation of aeromagnetic maps; Pseudo-Gravimetric Anomalies : Geophysics, vol. 22, no. 2, p. 359-383.
7. Hasegawa, H., 1967, A new method for numerical calculations of Pseudo-gravimetric anomalies : Butsuri-tanko (Geophysical Exploration), vol. 20, no. 5, p. 199-207.
8. Ogawa, K., 1977, A computer interpretation method for profiles of total intensity magnetic fields using a linear technique : Butsuri-tanko (Geophysical Exploration), vol. 30, no. 4 p. 218-228.

